Since January 2020 Elsevier has created a COVID-19 resource centre with free information in English and Mandarin on the novel coronavirus COVID-19. The COVID-19 resource centre is hosted on Elsevier Connect, the company's public news and information website.

Article

Cell Reports

Structural Definition of a Neutralization-Sensitive Epitope on the MERS-CoV S1-NTD

Graphical Abstract

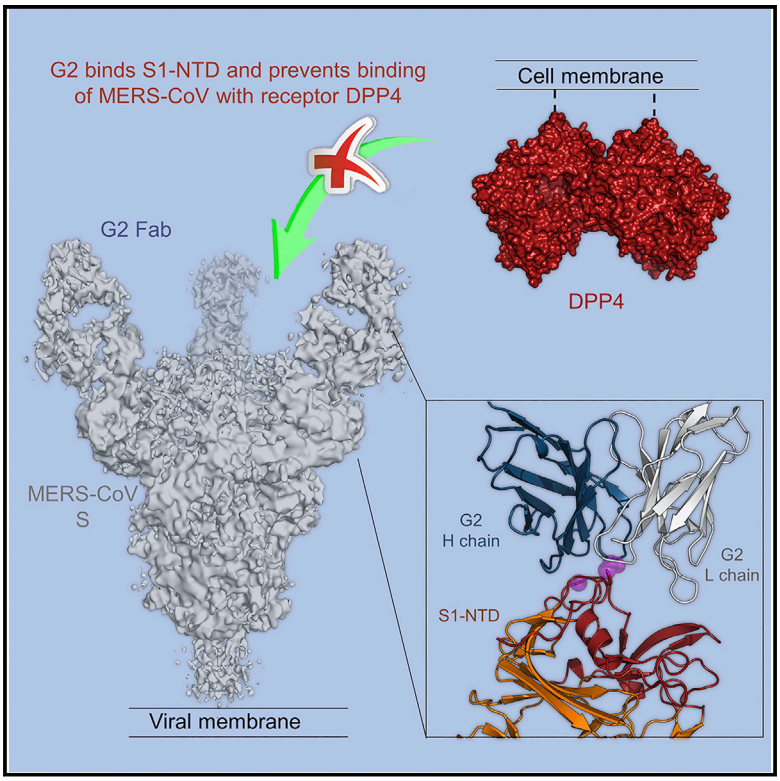

Authors

Nianshuang Wang, Osnat Rosen, Lingshu Wang, ..., Andrew B. Ward, Barney S. Graham, Jason S. McLellan

Correspondence

jmclellan@austin.utexas.edu

In Brief

Wang et al. report the structural and functional characterization of the Middle East respiratory syndrome coronavirus (MERS-CoV)-neutralizing antibody G2. G2 recognizes a conserved epitope on the MERS-CoV S1 N-terminal domain (S1-NTD) and neutralizes MERS-CoV by interfering with binding to host receptor dipeptidyl peptidase-4 (DPP4). The findings are relevant for understanding the viral attachment mechanism and for the development of S1-NTD-based vaccines.

Highlights

- The epitope for the neutralizing antibody G2 is confined to the apex of the MERS-CoV S1-NTD
- G2 epitope is relatively well conserved
- G2 IgG and Fab both neutralize pseudotyped and authentic MERS-CoV
- G2 neutralizes by preventing the binding of DPP4 to trimeric S protein

Wang et al., 2019, Cell Reports *28*, 3395–3405
September 24, 2019
https://doi.org/10.1016/j.celrep.2019.08.052

CellPress

Cell Reports
Article

Structural Definition of a Neutralization-Sensitive Epitope on the MERS-CoV S1-NTD

Nianshuang Wang,[1] Osnat Rosen,[2,6] Lingshu Wang,[2] Hannah L. Turner,[3] Laura J. Stevens,[4] Kizzmekia S. Corbett,[2] Charles A. Bowman,[3] Jesper Pallesen,[3] Wei Shi,[2] Yi Zhang,[2] Kwanyee Leung,[2] Robert N. Kirchdoerfer,[3] Michelle M. Becker,[4] Mark R. Denison,[4,5] James D. Chappell,[4] Andrew B. Ward,[3] Barney S. Graham,[2] and Jason S. McLellan[1,7,*]

[1]Department of Molecular Biosciences, The University of Texas at Austin, Austin, TX 78712, USA
[2]Vaccine Research Center, National Institute of Allergy and Infectious Diseases, NIH, Bethesda, MD 20892, USA
[3]Department of Integrative Structural and Computational Biology, The Scripps Research Institute, La Jolla, CA 92037, USA
[4]Department of Pediatrics, Vanderbilt University School of Medicine, Nashville, TN 37232, USA
[5]Department of Pathology, Microbiology, and Immunology, Vanderbilt University School of Medicine, Nashville, TN 37232, USA
[6]Present address: Department of Biotechnology, Israel Institute for Biological Research, Ness-ziona, Israel
[7]Lead Contact
*Correspondence: jmclellan@austin.utexas.edu
https://doi.org/10.1016/j.celrep.2019.08.052

SUMMARY

Middle East respiratory syndrome coronavirus (MERS-CoV) emerged into the human population in 2012 and has caused substantial morbidity and mortality. Potently neutralizing antibodies targeting the receptor-binding domain (RBD) on MERS-CoV spike (S) protein have been characterized, but much less is known about antibodies targeting non-RBD epitopes. Here, we report the structural and functional characterization of G2, a neutralizing antibody targeting the MERS-CoV S1 N-terminal domain (S1-NTD). Structures of G2 alone and in complex with the MERS-CoV S1-NTD define a site of vulnerability comprising two loops, each of which contain a residue mutated in G2-escape variants. Cell-surface binding studies and *in vitro* competition experiments demonstrate that G2 strongly disrupts the attachment of MERS-CoV S to its receptor, dipeptidyl peptidase-4 (DPP4), with the inhibition requiring the native trimeric S conformation. These results advance our understanding of antibody-mediated neutralization of coronaviruses and should facilitate the development of immunotherapeutics and vaccines against MERS-CoV.

INTRODUCTION

Middle East respiratory syndrome coronavirus (MERS-CoV) is a zoonotic coronavirus first identified in Saudi Arabia in 2012 (van Boheemen et al., 2012; Zaki et al., 2012). MERS-CoV can cause severe acute respiratory disease in humans with symptoms including fever, cough, and shortness of breath (WHO, 2018). Through the end of 2018, the World Health Organization (WHO) has been notified of 2,266 laboratory-confirmed cases of MERS-CoV infection from 27 countries, with most cases occurring in the Middle East (WHO, 2018). The MERS-CoV case-fatality rate for laboratory-confirmed severe disease is 36%, with the number of deaths exceeding 800. MERS-CoV likely originated from bats, with camels functioning as a secondary or intermediate host (Azhar et al., 2014; Mohd et al., 2016). Small clusters of infections in several countries suggested that limited human-to-human transmission can occur through close contact (Ki, 2015; Oboho et al., 2015). Due to the ongoing circulation, high pathogenicity, and capacity for inter-human transmission associated with MERS-CoV, there is a persistent concern about a possible pandemic. Because no specific antiviral drugs or protective vaccines are currently available, efficient countermeasures against this virus are urgently needed.

The surface of coronavirus virions is decorated with the large trimeric spike (S) glycoprotein, which mediates cell entry (Gierer et al., 2013; Li, 2016). The MERS-CoV S glycoprotein is synthesized as a single-chain precursor that is subsequently cleaved by furin-like host proteases to generate the S1 and S2 subunits (Millet and Whittaker, 2014). The mature S protein is a homotrimer of non-covalently associated S1 and S2 subunits whereby a trimer of S1 acts as a fusion-suppressive cap and sits atop a trimer of S2 subunits. Binding of S1 to the host receptor dipeptidyl peptidase-4 (DPP4) (Lu et al., 2013; Raj et al., 2013; Wang et al., 2013) initiates a large irreversible conformational change of S2, which mediates fusion of the viral and host-cell membranes. Cryoelectron microscopy (cryo-EM) structures of various β-coronaviruses (Gui et al., 2017; Kirchdoerfer et al., 2016; Pallesen et al., 2017; Shang et al., 2018a, 2018b; Walls et al., 2016a, 2016b; Xiong et al., 2018; Yuan et al., 2017) have revealed a four-domain architecture of S1 including an N-terminal domain (NTD), a C-terminal domain (CTD), and subdomains I and II. S1-NTD or S1-CTD can function as the receptor-binding domain (RBD) depending on the specific coronavirus. Most β-coronaviruses, including severe acute respiratory syndrome-CoV (SARS-CoV) (Li et al., 2003, 2005) and MERS-CoV (Lu et al., 2013; Raj et al., 2013; Wang et al., 2013), use the S1-CTD to bind to their functional receptor, whereas some lineage A β-coronaviruses, such as mouse hepatitis virus (MHV) (Peng et al., 2011) and bovine coronavirus (BCoV) (Peng et al., 2012), bind receptors using the S1-NTD.

Prefusion S1 proteins from some coronaviruses, including human coronavirus HKU1 (HCoV-HKU1) (Kirchdoerfer et al., 2016) and MHV (Walls et al., 2016a), fold into a well-packed symmetric trimer with NTDs and CTDs tightly interacting with each other. In this conformation, the receptor-binding surface on the CTDs is mostly occluded within the internal surface of the trimer. Conversely, prefusion SARS-CoV (Gui et al., 2017; Yuan et al., 2017) and MERS-CoV (Pallesen et al., 2017; Yuan et al., 2017) S1 proteins adopt dynamic open and closed conformations, wherein each of the three S1-CTDs adopt either a compact "down" conformation that buries the receptor-binding surface, or an "up" conformation that facilitates binding with host-cell receptors. It has been hypothesized that these conformations exist in an equilibrium, with receptor binding to the up conformation resulting in a three CTD up arrangement that is unstable, resulting in dissociation of S1 and refolding of S2 (Gui et al., 2017; Pallesen et al., 2017; Song et al., 2018; Walls et al., 2019; Yuan et al., 2017).

Coronavirus S1-NTDs adopt a three-layer structure, with a core region formed by a galectin-like β sandwich fold, a top region above the core that is commonly used by some lineage A β-coronaviruses to bind proteins or glycan receptors, and a bottom conserved region that stretches out to connect with the S1-CTD (Peng et al., 2011). Structures of MERS-CoV S1-NTD have been reported previously (Pallesen et al., 2017; Yuan et al., 2017), but specific interactions with host-cell factors have not been well characterized. Recent studies have suggested that CEACAM5 (Chan et al., 2016), GRP78 (Chu et al., 2018), and sialic acid (Li et al., 2017) may serve as important attachment factors prior to DPP4 binding, and these interactions may be mediated by the S1-NTD.

As the main protein on the surface of the coronavirus virion, the S protein is the key target for protective antibody responses (Li, 2016; Modjarrad et al., 2016). Many neutralizing antibodies targeting the MERS-CoV S1-CTD, which is the RBD, have been isolated and characterized (Corti et al., 2015; Jiang et al., 2014; Li et al., 2015; Tang et al., 2014; Ying et al., 2014), and structural studies have revealed that their epitopes overlap with the DPP4-binding surface, thereby providing a structural basis for neutralization. Besides the immunodominant RBD, the S1-NTD has also been shown to induce protective antibody responses in a mouse model (Jiaming et al., 2017). Neutralizing antibodies targeting MERS-CoV S1-NTD have been reported, including human antibody CDC2-A2, murine antibodies G2 and 5F9, and macaque antibodies FIB-H1 and JC57-13 (Chen et al., 2017; Wang et al., 2015, 2018). Of these antibodies, G2 is the most potent, with broad neutralization potential against an array of MERS-CoV strains (Wang et al., 2018). Additionally, G2 and other NTD-specific MERS-CoV antibodies have been shown to confer protection against lethal challenge in animal models (Wang et al., 2018). However, the lack of structural information for G2 has hindered the definition of its epitope and determination of its mechanism of action.

To address this knowledge gap, we initiated a series of comprehensive studies. Here, we report the crystal structures of G2 Fab alone and bound to the MERS-CoV S1-NTD, as well as the results from biochemical, biophysical, and cell-based assays. These studies define a site of vulnerability on the MERS-CoV spike and elucidate a mechanism of neutralization that involves inhibition of attachment to DPP4.

RESULTS

The G2 Epitope Is Confined Solely to the S1-NTD

We conducted surface plasmon resonance (SPR) experiments to characterize the interaction between G2 Fab and MERS-CoV S1-NTD (Figure 1A), as well as the interaction between G2 Fab and the prefusion-stabilized MERS-CoV S ectodomain (MERS-CoV S-2P) (Pallesen et al., 2017) (Figure 1B). The affinities of G2 Fab for S1-NTD and MERS-CoV S-2P were very similar, with K_Ds of 28.0 and 30.3 nM, respectively. The binding kinetics were also in good agreement, indicating that the G2 epitope is confined to the S1-NTD.

To more precisely localize the G2 epitope on the S1-NTD, we performed *in vitro* selection for G2-escape variants by serial passage of recombinant MERS-CoV strain EMC/2012 in Vero 81 cell cultures (Scobey et al., 2013) supplemented with progressively escalating concentrations of G2 immunoglobulin G (IgG). After 10 passages, 15 G2-resistant MERS-CoV isolates were plaque cloned and the mutations were analyzed. All 15 clones contained either an S28F or G198D substitution (Table S1), suggesting that these two residues are crucial for G2 binding. To test this hypothesis, we generated MERS-CoV S-2P variants harboring the S28F or G198D substitutions. SPR measurements revealed that the S28F or G198D substitutions completely abolished binding to G2 Fab at the concentrations tested (Figures 1C and 1D). We next generated pseudotyped lentiviruses bearing the mutant MERS-CoV S glycoproteins (S28F or G198D) to assess the effect of these substitutions on the neutralizing activity of G2 IgG. As expected, G2 IgG potently neutralized pseudoviruses bearing wild-type (WT) S protein, whereas G2 IgG poorly neutralized the pseudoviruses harboring the escape mutations, with a maximum neutralized fraction below 45% (Figure 1E). We additionally verified the neutralizing ability of G2 IgG against the recombinant MERS-CoV strain EMC/2012 (Almazán et al., 2013) and the G198D variant in a biosafety level 3 (BSL-3) setting. G2 IgG neutralized authentic MERS-CoV with an EC_{50} = 0.12 nM, whereas the ability of G2 IgG to neutralize the G198D variant was barely detectable until we raised the concentration to 10 μM (Figure 1F). These results indicate that the G2 epitope is localized to a surface on the S1-NTD near residues Ser28 and Gly198.

The G2 Epitope Is Primarily Localized to Two Loops at the Top of S1-NTD

To precisely define the G2 epitope, we determined the crystal structures of G2 Fab alone and in complex with MERS-CoV S1-NTD. G2 Fab formed crystals in space group $P2_1$ that diffracted X-rays to 2.1-Å resolution. Phasing by molecular replacement revealed four Fab molecules per asymmetric unit. After iterative rounds of model building and refinement, the final model had an R/R_{free} = 18.1%/22.5% (Table S2). Crystallization of G2 Fab in complex with the S1-NTD proved difficult and necessitated exploration of different expression and purification strategies. Ultimately, crystals of the complex were obtained in space group $P2_1$ that diffracted X-rays to 2.3-Å resolution. The

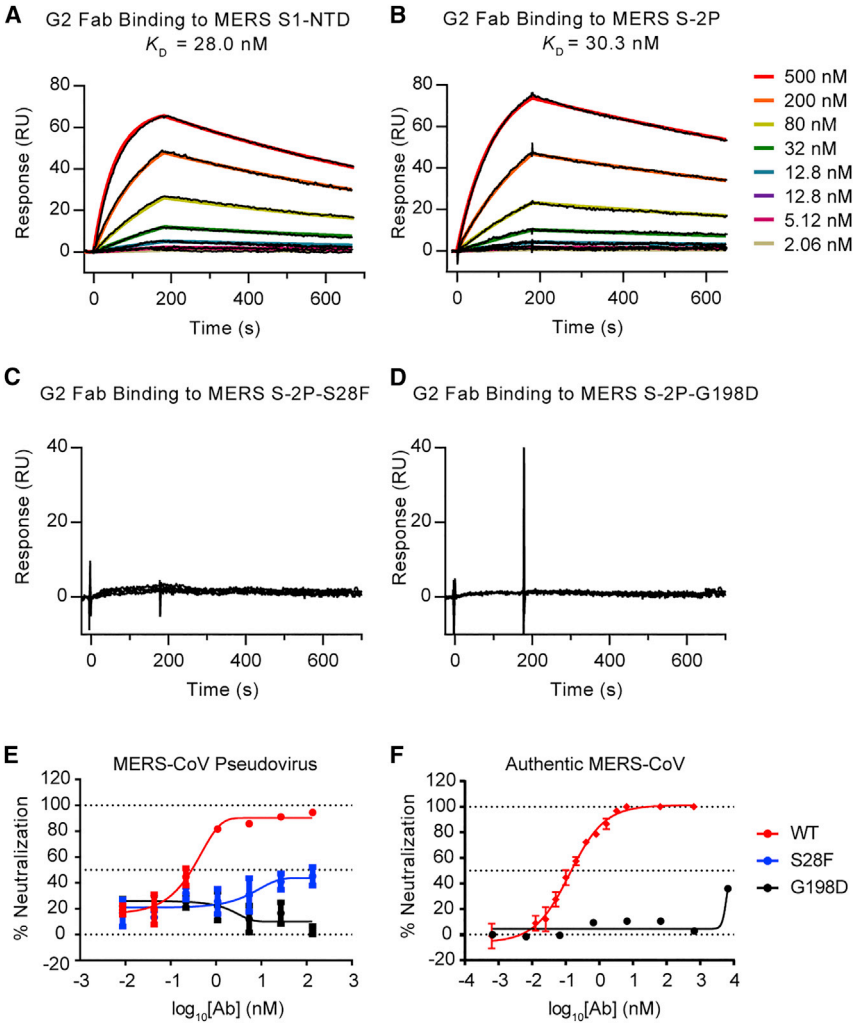

Figure 1. Two Selected G2-Escape Mutations and Their Impact on G2 Binding and Neutralization

(A–D) Binding of G2 Fab to immobilized (A) MERS-CoV S1-NTD, (B) MERS-CoV S-2P, (C) MERS-CoV S-2P-S28F, and (D) MERS-CoV S-2P-G198D measured by surface plasmon resonance (SPR). The same concentration series of G2 Fab was used in (A)–(D). Best global fit of the data to a 1:1 binding model is shown as colored lines.

(E) Neutralization activity of G2 IgG was measured against pseudotyped lentivirus bearing MERS-CoV S (WT) and two variants (S28F and G198D). Percent neutralization of WT (red), S28F (blue), and G198D (black) S pseudovirions at the different antibody concentrations is shown. Data points represent the mean of three technical replicates with standard errors.

(F) Neutralization activity of G2 IgG was measured against authentic MERS-CoV (WT) and the G198D variant. Percent neutralization of WT (red) and G198D (black) MERS-CoV at the different antibody concentrations is shown. Data points for the WT virus represent the mean of two technical replicates.

molecular replacement solution contained two molecules of the complex per asymmetric unit, and iterative rounds of model building and refinement produced a final model with an R/R_{free} = 18.0%/21.3%.

The structure of the MERS-CoV S1-NTD is similar to that of other coronaviruses and can be separated into top, core, and bottom regions (Figure 2A). The MERS-CoV S1-NTD core contains a β sandwich structure formed by two β sheets containing a total of 11 β strands (Figure 2B, labeled β1-β11), providing a scaffold to support the top and bottom regions. Stretching out from β5, a loop (residues 189-202) designated loop2 spirals 540° perpendicularly to the β sheet, like a right-handed pseudo-helix, and comprises the majority of the G2 binding interface (~384 Å^2). A disulfide bond between Cys30 and Cys195 connects loop2 with an *N*-terminal loop (residues 18–33) designated loop1, which contributes the remaining binding interface with G2 (~295 Å^2) (Figures 2B and 2C).

Four of the six G2 complementarity-determining regions (CDRH1, CDRH2, CDRH3, and CDRL3) are involved in binding to the S1-NTD (Figure 2D). CDRL3 interacts with loop1, whereas the heavy-chain CDRs interact with loop2, except for one hydrogen bond formed between CDRH3 residue Ser97 and S1-NTD loop1 residue Ser28. G2 heavy-chain residues Tyr33, Thr54, and Ser97 form hydrogen bonds with main-chain atoms on loop2, whereas heavy-chain residues Trp50 and Tyr52 interact with side chains of loop1 residues Ser191 and Asn199, respectively. The interaction between the G2 light chain and loop1 is mediated by three residues on CDRL3 (Ser91, Glu92, and Glu93) and two residues on loop1 (Lys27 and Ser28). Loop1 residue Lys27 forms two salt bridges with Glu92 and Glu93 on CDRL3, whereas Ser28 forms hydrogen bonds with main-chain atoms of CDRL3 residues Ser91 and Glu92.

There are eight *N*-linked glycosylation sites within the S1-NTD. As the crystallized protein was not treated with glycosidases, electron density for large glycan moieties can be observed on several glycosylation sites. However, none of these glycosylation sites are within the G2 binding interface (Figure S1A). Thus, it is unlikely that G2 binding is dependent on the presence of *N*-linked glycans. To verify, SPR studies confirmed that deglycosylated S1-NTD retained a similar affinity to G2 as glycosylated S1-NTD (Figure S1B).

The structure is consistent with the G2-escape data, which showed that MERS-CoV cultured under G2 selection accumulates substitutions S28F and G198D at the G2 binding interface (Table S1). Based on the structure, we predict that the S28F substitution would largely eliminate the hydrophilic interactions between loop1 and CDRL3. The G198D substitution would introduce a long side chain leading to a steric clash that would impair the interaction. In addition to these two escape mutations, we

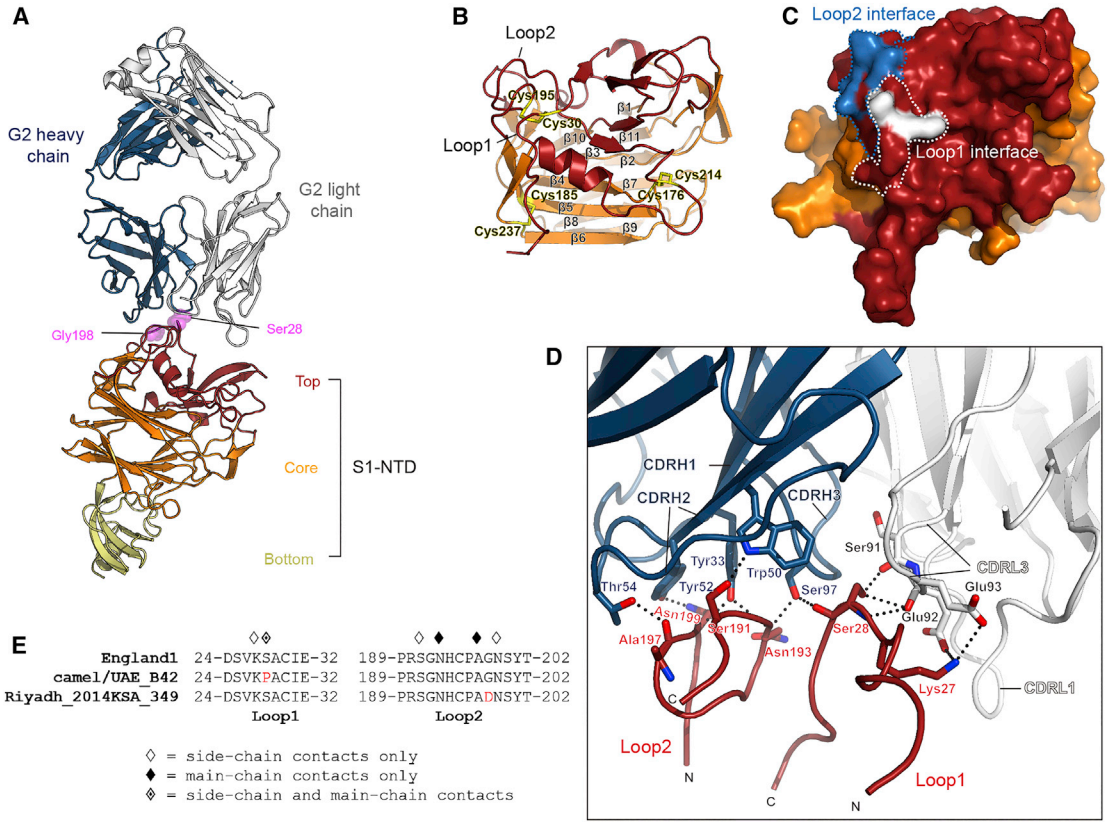

Figure 2. Structure of G2 Fab Complexed with MERS-CoV S1-NTD

(A) Overall structure of the complex. G2 heavy and light chains are colored dark blue and white, respectively. S1-NTD is separated into top (red), core (orange), and bottom (yellow) regions. Residues Ser28 and Gly198 are shown as semi-transparent molecular surfaces.

(B) The structure of S1-NTD top region is presented in ribbon representation. The 11 β strands in the core region are labeled β1-β11. Disulfide bonds are drawn as yellow sticks.

(C) The structure of S1-NTD top region is presented as a molecular surface, viewed in the same orientation as in (B). Surfaces on loop1 and loop2 buried at the interface with G2 are encircled by a dotted line and residues forming hydrogen bonds with G2 are colored white and blue, respectively.

(D) G2 contacts two loops (loop1 and loop2) on the S1-NTD top region. Antibody complementarity-determining regions (CDRs) involved in the binding are labeled. Residues contributing to the interaction are shown in a stick representation. Hydrogen bonds and salt bridges are depicted as black dotted lines.

(E) Linear sequences of loop1 and loop2. S1-NTD residues that make hydrogen bonds to G2 are denoted with symbols. Two G2-escape mutations (S28P and G198D) naturally occurring in S proteins from two different MERS-CoV strains (camel/UAE_B42 and Riyadh_2014KSA_349, respectively) are colored red.

further probed the interface by introducing single mutations K27A or S191A into the S1-NTD. As expected from the structure, either of these two substitutions largely abolished the binding to G2 Fab (Figure S2A).

The G2 Epitope Is Relatively Conserved

Previous neutralization data demonstrated that G2 IgG can neutralize pseudoviruses with S proteins from eight different MERS-CoV strains with inhibitory concentration $(IC)_{50}$ values ranging from 0.010 to 0.028 μg/ml (Wang et al., 2018). This is in contrast to other S1-NTD-specific antibodies, like A2 and JC57-13, which showed weaker neutralizing potency. We analyzed the S1-NTD sequences from all eight tested strains and identified amino acid differences at seven positions. However, none of these are involved in the interaction with G2 (Figure S2B).

We additionally analyzed all available MERS-CoV S sequences in GenBank. Most of the G2-interacting residues, including Lys27, Ser191, Asn193, Ala197, and Asn199, are conserved among all 232 sequences, explaining why G2 IgG can broadly neutralize MERS-CoV strains. Interestingly, we did find some MERS-CoV strains with substitutions at Ser28 or Gly198 (Figure 2E), the two residues that were substituted in escape variants under *in vitro* G2 selection. Eight sequences (ASU90362, ASU90142, ASU89988, ASU91208, ASU91284, ASU90186, ASU90010, and ASU89966) isolated from camels (Yusof et al., 2017), along with one sequence isolated from a patient in 2015 (ALJ54461) (Assiri et al., 2016), harbor a S28P substitution. One human MERS-CoV sequence isolated in 2014 (Drosten et al., 2015) is the only one that harbors a G198D mutation. We tested an S1-NTD construct bearing the S28P substitution for binding to G2 Fab. The affinity was ~10-fold lower compared to the affinity of WT S1-NTD (Figure S2A). The natural occurrence of S28P and G198D may indicate that MERS-CoV is under selective pressure exerted by host G2-like antibody responses.

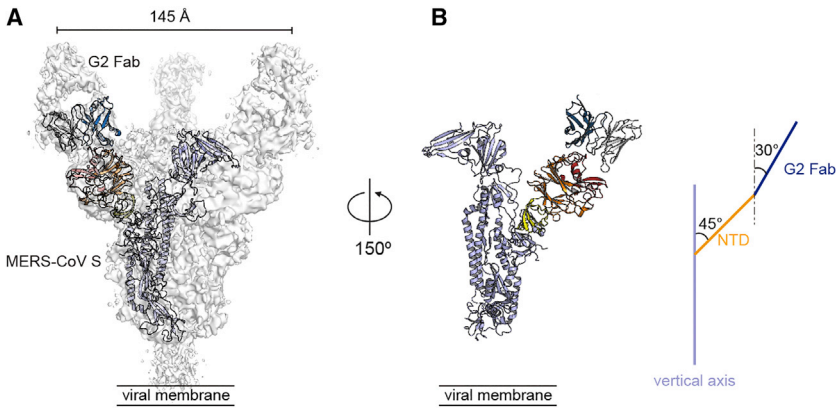

Figure 3. G2 Binding to the Prefusion MERS-CoV Spike

(A) Cryo-EM structure of uncleaved MERS-CoV S0 ectodomain in complex with G2 Fab as viewed along the viral membrane. A single protomer of the trimeric S protein is shown in ribbon representation, with S1-NTD and G2 colored the same as in Figure 2 and the rest of S colored light blue. See also Figures S3C and S3D.

(B) Structural model of G2 Fab bound to one MERS-CoV S protomer. The angles of the S1-NTD and G2 Fab to the 3-fold axis are depicted.

G2 Binding to the Prefusion Spike

To further investigate G2 binding in the context of the MERS-CoV S trimer, we purified the MERS-CoV S0 ectodomain in complex with G2 Fab and performed negative-stain EM analysis. 2D classification suggested that the sample was heterogeneous, and postfusion rod-like particles were abundant (Figure S3A), suggesting that G2 Fab is not able to prevent the prefusion-to-postfusion transformation of S0 ectodomains in solution. We then generated a 24-Å-resolution 3D reconstruction. The NTD-G2 Fab crystal structure was superimposed onto the prefusion MERS-CoV S structure (PDB: 5W9J) to generate a model, which fit well into the reconstruction (Figure S3B), indicating that G2 Fab binding does not induce substantial conformational changes in the MERS-CoV S trimer. Note that density for the RBD is missing due to the intrinsic dynamics of the RBD (Gui et al., 2017; Pallesen et al., 2017; Yuan et al., 2017).

To further investigate the interaction of G2 with the MERS-CoV S trimer, we determined a 4.2-Å cryo-EM structure of a MERS-CoV S0-G2 Fab complex (Figures 3A, S3C, and S3D; Table S3). The MERS-CoV S1 NTDs reside on the periphery of the S1 trimer, flared out approximately 45° to the 3-fold axis. The G2 interface is situated at the apex of the S protein, and binding of G2 Fab elongates the S1-NTD axis to form three legs of an inverted "tripod" structure, with a 15° tilt toward the 3-fold axis (Figure 3B). The distance between two bound Fabs is 110 Å at the binding interface and 145 Å at the distal end of the Fab (Figure 3A). There are no substantial conformational changes in the trimer resulting from G2 binding.

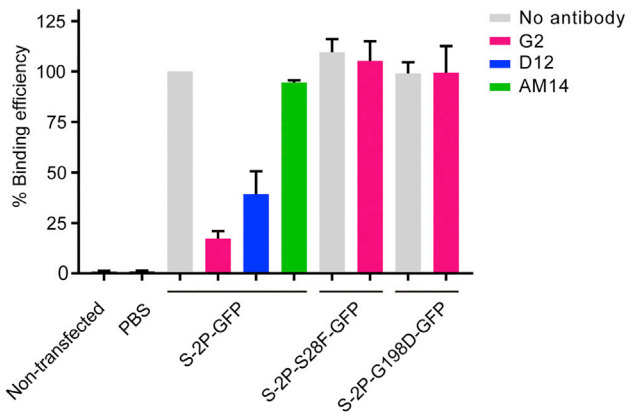

Figure 4. G2 IgG Prevents the Binding of MERS-CoV S Protein to DDP4-Expressing Cells

Normalized binding efficiency of GFP-tagged MERS-CoV S-2P proteins to DPP4-expressing FreeStyle 293F cells in the presence or absence of IgGs was calculated from median fluorescence intensity (MFI) values. FreeStyle 293-F cells were transfected with a plasmid encoding full-length DPP4 60 h before the experiment. Non-transfected cells (NTs) incubated with MERS-CoV S-2P, as well as transfected cells incubated with PBS, were used as negative controls. AM14 is an irrelevant RSV F-specific neutralizing antibody used as another negative control. Bar graph shows the mean and error bars indicate the standard deviation (n = 3 biologically independent experiments with two technical replicates).

G2 Prevents S Protein Binding to the Cell Surface

The binding of G2 Fab to the apex of the spike, where interactions with host-cell factors such as DPP4 occur, suggested that G2 IgG may interfere with the attachment step during cell entry. To test this hypothesis, we performed cell-surface binding assays. As shown in Figure 4, GFP-labeled MERS-CoV S-2P strongly bound to DPP4-transfected HEK293 cells. This binding was substantially reduced by pre-incubation of MERS-CoV S-2P with a 5-fold molar excess of G2 IgG or an RBD-specific antibody, D12. Interestingly, G2 reduced MERS-CoV S-2P binding more than D12 did, even though they have similar neutralizing potencies (Wang et al., 2015). MERS-CoV S-2P variants with substitutions S28F or G198D bound to cells at levels similar to those observed for WT MERS-CoV S-2P. However, in contrast to WT MERS-CoV S-2P, these two variants were insensitive to G2 IgG and maintained high-level cell-surface binding even in the presence of excess G2 IgG. Collectively, these data demonstrate that G2 IgG prevents attachment of MERS-CoV S to cells expressing DPP4.

G2 Fab Neutralizes but Not through a Direct Steric Clash with DPP4

The binding of MERS-CoV S to DPP4 requires the RBDs to rotate upward to expose the receptor binding surface (Figure 5A). Presumably, antibodies can block the receptor-binding process by inhibiting RBD movement or DPP4 attachment. To gain insight into the mechanism of G2 attachment inhibition,

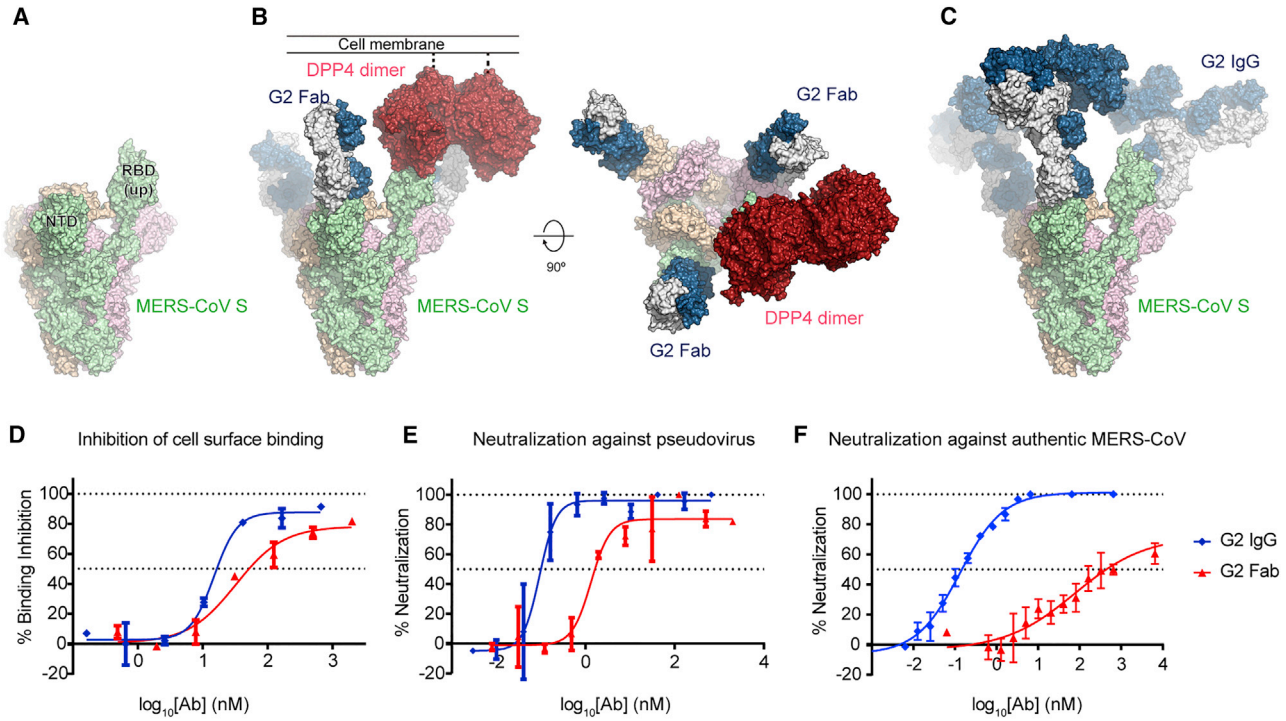

Figure 5. Comparison of DPP4 Binding-Inhibition and Neutralization Activity of G2 IgG versus Fab

(A–C) Structural models of MERS-CoV S trimers with a single RBD in the up conformation (A) unbound, (B) bound to G2 Fab and DPP4, and (C) bound to G2 IgG. Models were generated in PyMOL based on superimposed structures of MERS-CoV S (PDB: 5W9H), RBD-DPP4 complex (PDB: 4L72), mouse IgG1 (PDB: 1IGY), and the S1-NTD–G2 structure described in this paper. MERS-CoV S protomers are colored green, pink, and orange, with the green protomer in the "RBD up" conformation. The DPP4 dimer is colored red, whereas the G2 heavy and light chains are colored blue and white, respectively.

(D) Inhibition of soluble MERS-CoV S-2P binding to DDP4-expressing cells as a function of IgG or Fab concentration. The mean of duplicate measurements is plotted. Error bars represent SEM.

(E) Neutralization of MERS-CoV pseudoviruses as a function of IgG or Fab concentration. The mean of duplicate measurements is plotted. Error bars represent SEM.

(F) Neutralization of authentic MERS-CoV as a function of IgG or Fab concentration. The mean of duplicate measurements is plotted. The IgG data are the same as those plotted in Figure 1F.

we superimposed G2 and DPP4 onto the MERS-CoV S structure using the S1-NTD-G2 Fab structure presented here and the previously determined DPP4-RBD structure (Lu et al., 2013; Wang et al., 2013). Surprisingly, the structural model indicates that G2 Fab would not prevent movement of the RBD nor sterically clash with DPP4 (Figure 5B). However, a steric clash would be predicted to occur between MERS-CoV S and the host-cell membrane if G2 IgG were bound (Figure 5C), and the bivalent G2 IgG could also possibly cross-link two adjacent MERS-CoV S trimers, resulting in restricted access for DPP4.

To determine whether the G2 Fab, rather than the larger IgG, was sufficient for activity, the binding inhibition and neutralizing ability of G2 Fab were evaluated. Consistent with our previous data (Wang et al., 2018; Rosen et al., 2019), G2 IgG displayed strong inhibition of soluble MERS-CoV S binding to DPP4-expressing BHK21 cells with an IC_{50} of 15 nM (Figure 5D), as well as strong neutralization of MERS-CoV S-containing pseudoviruses with an IC_{50} of 0.09 nM (Figure 5E). G2 Fab also inhibited cell binding (IC_{50} = 32.3 nM) (Figure 5D) and neutralized MERS-CoV S-containing pseudoviruses (IC_{50} = 1.33 nM), although not as well as G2 IgG (Figure 5E). G2 Fab also neutralized authentic MERS-CoV in a dose-dependent manner, but as we observed with the pseudoviruses, the neutralizing activity of the Fab was not as strong as the IgG (Figure 5F). Based on these data, we conclude that G2 Fab is sufficient for neutralization and blocking attachment of MERS-CoV S to DPP4-expressing cells, but likely not by clashing with DPP4 nor restricting exposure of the RBDs.

G2 Neutralizes by Preventing the Binding of Trimeric S Protein with DPP4

Although it is possible that the S1-NTD contributes to the cell-surface attachment process by directly binding one or more attachment factors, the RBD plays the predominant role in this event by strongly binding to the functional receptor DPP4. We hypothesized that G2 blocks cell-surface attachment by indirectly inhibiting the RBD-DPP4 interaction. To test this, we investigated cell-surface binding of soluble DPP4 to membrane-anchored MERS-CoV S1 (S1-TM), full-length S-WT (S-WT-FL), or full-length S-2P (S-2P-FL) in the presence or absence of excess G2 Fab. We observed that DPP4 bound well to cells

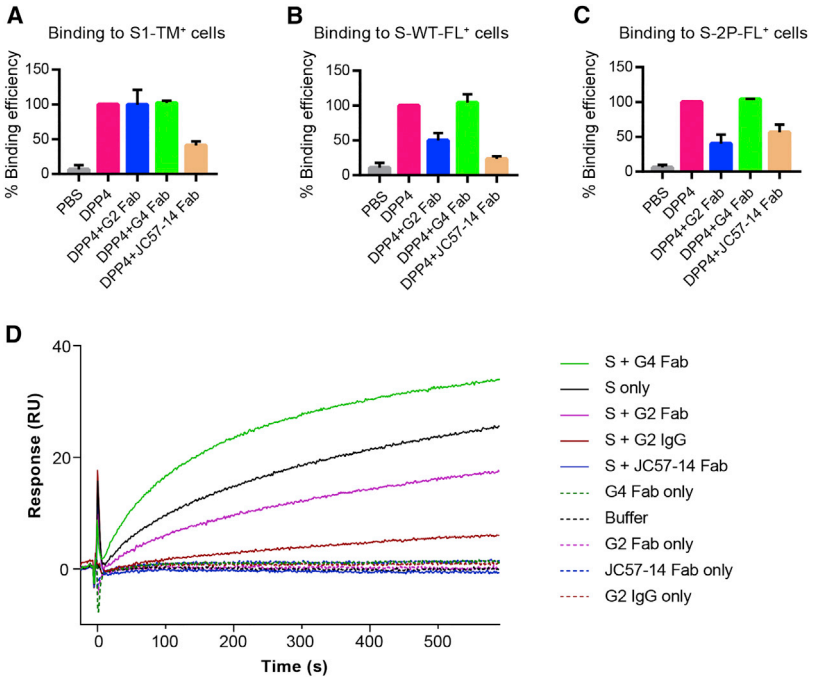

Figure 6. G2-Mediated Inhibition of DPP4 Binding to MERS-CoV S Depends on the Oligomeric State of the Spike

(A–C) Normalized binding efficiency of DPP4, in the presence or absence of Fab, to cells transfected with plasmids encoding (A) membrane-anchored S1 (S1-TM), (B) full-length S-WT (S-WT-FL), and (C) full-length S-2P (S-2P-FL). Cells incubated with PBS were used as negative controls. Bar graph shows the mean and error bars indicate the standard deviation (n = 3 biologically independent experiments with two technical replicates). (D) Surface plasmon resonance competition assay. Response curves for MERS-CoV S-2P, alone or in the presence of a 5-fold molar excess of indicated Fabs or IgGs, passed over an immobilized DPP4 ectodomain. The curves for S-2P or S-2P supplemented with Fab or IgG are shown with a solid line, whereas control curves for samples without S-2P are shown with a dotted line.

transfected with each of the three S protein constructs (Figures 6A–6C), as expected. As a positive antibody control, RBD-specific JC57-14 Fab strongly inhibited binding of DPP4 to each of the transfected cells by directly competing with DPP4 for RBD binding (Wang et al., 2018). As a negative antibody control, the S2-specific G4 Fab (Pallesen et al., 2017; Wang et al., 2015) exhibited no binding inhibition. When G2 Fab was tested, a different binding-inhibition pattern was observed. G2 Fab prevented binding of DPP4 to cells expressing trimeric full-length S-WT or S-2P, but allowed binding of DPP4 to cells expressing a membrane-tethered form of S1 that is predicted to be monomeric (Figures 6A–6C). These data indicate that DPP4 binding inhibition by G2 Fab depends on the intact trimeric conformation of the S protein.

To exclude the possibility that unknown cell-surface factors may play roles in G2's inhibition of DPP4 binding to MERS-CoV S trimers, we performed an SPR competition assay using purified proteins (Figure 6D). We captured DPP4 onto the SPR chip and then flowed over MERS-CoV S-2P protein or MERS-CoV S-2P protein supplemented with a 5-fold molar excess of different Fabs. MERS-CoV S-2P in the absence of Fabs bound well to the captured DPP4 (black curve). MERS-CoV S-2P supplemented with the RBD-specific JC57-14 Fab displayed no binding (blue curve), confirming the strong competition between JC57-14 Fab and DPP4 for binding to the RBD. MERS-CoV S-2P supplemented with the S2-specific G4 Fab displayed a higher response curve than MERS-CoV S-2P alone due to the added mass of the bound G4 Fab and its lack of binding inhibition. MERS-CoV S-2P supplemented with G2 Fab displayed substantially lower binding to the captured DPP4 than either the MERS-CoV S-2P supplemented with G4 Fab or MERS-CoV S2-P alone (purple curve), confirming that G2 interferes with DPP4 binding to trimeric MERS-CoV S. G2 IgG reduced the binding of MERS-CoV S-2P even further (red curve), despite the increased mass of the IgG compared to the Fab. Unlike JC57-14 Fab, neither G2 Fab nor G2 IgG blocked DPP4 binding completely, suggesting that G2 uses an indirect mechanism of inhibition.

DISCUSSION

Around 20 different monoclonal antibodies have been isolated that can neutralize MERS-CoV, with the majority targeting the RBD. With the exception of the S2-specific antibody G4, the other non-RBD-directed MERS-CoV neutralizing antibodies that have been isolated are S1-NTD specific, including G2 and 5F9 from mice, JC57-13 and FIB-H1 from macaques, and CDC2-A2 from a human (Chen et al., 2017; Wang et al., 2015, 2018). S1-NTD-specific neutralizing antibodies have also been isolated against SARS-CoV (Coughlin et al., 2009; Greenough et al., 2005; Rockx et al., 2008), including 4D4, 68, S132, and S228.11. Thus, for SARS-CoV and MERS-CoV, the S1-NTD is a common site of antibody vulnerability. Despite a lack of structural characterization, studies with these antibodies provide some insight into their neutralizing mechanism. Antibody 4D4 was shown to bind the SARS S1-NTD fragment between residues 12 and 261 (Coughlin et al., 2009). 4D4 efficiently prevented viral entry when added after the binding of pseudovirus onto target cells, suggesting 4D4 is more likely to neutralize through disrupting a post-binding event instead of interfering with the cell attachment process. We also note that another MERS-CoV S1-NTD-specific neutralizing antibody, A2, does not compete with G2 (Wang et al., 2018), indicating that G2 and A2 recognize different epitopes on the S1-NTD. Thus, it is likely that S1-NTD-derived antibodies can neutralize through different mechanisms.

The molecular mechanisms regulating receptor binding and fusion activation of coronavirus spike proteins are currently the subject of active investigation in the field. Recent studies have

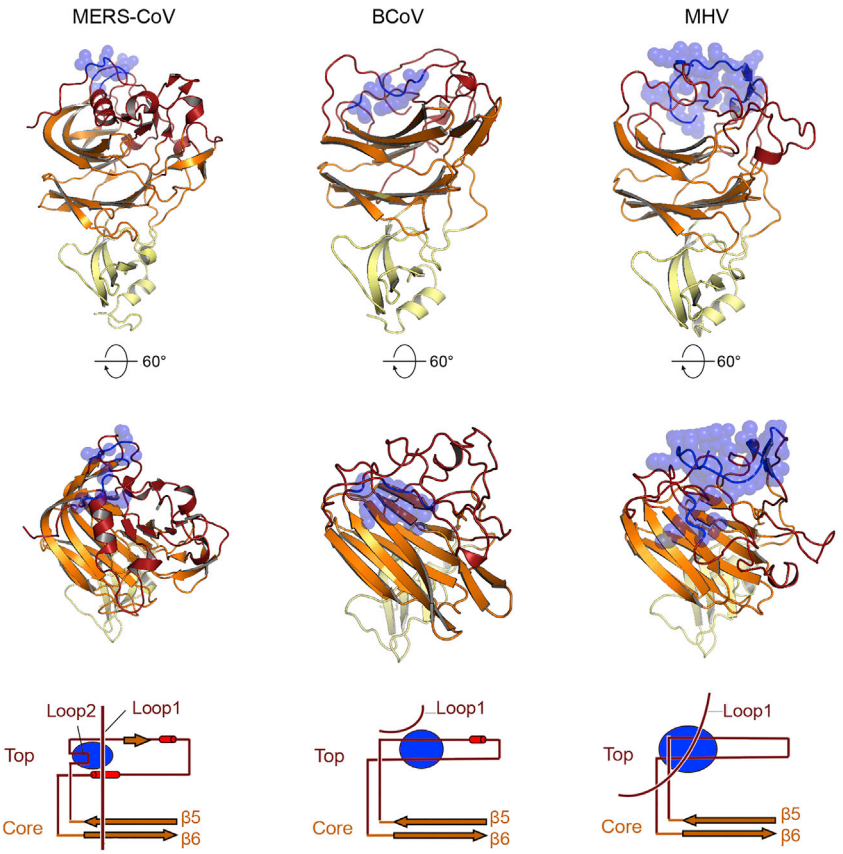

Figure 7. Comparison of the S1-NTD Top Region from MERS-CoV, BCoV, and MHV

S1-NTD is colored as in Figure 2 and depicted in ribbon representation in the top and middle rows. Residues interacting with G2 Fab, sialic acid, and CEACAM1 are shown as blue spheres on the MERS-CoV, BCoV, and MHV structures, respectively. Topology models of the S1-NTDs are shown in the bottom row, with β sheets depicted as arrows and α helices depicted as red cylinders. The binding surfaces described above are denoted with a blue oval. Figures were made based on the structure of MERS-CoV S1-NTD–G2 Fab described in this paper, BCoV S1-NTD (Peng et al., 2012) (PDB: 4H14), and MHV S (Peng et al., 2011) (PDB: 3JCL).

demonstrated that both receptor binding and proteolytic cleavage are required to shed S1 and allow refolding of S2 to the post-fusion state (Song et al., 2018; Walls et al., 2019). Our data suggest that the S1-NTD may play a role in regulating this finely tuned process, although the molecular details remain unknown. Upon binding the NTDs, the large bivalent G2 IgG would be able to generate a barrier at the virus-host interface to prevent attachment (Figure 5C). DPP4 has a short 11-residue stalk, which restricts its movement and access to the RBDs of a G2-bound S protein. This can reasonably explain the neutralization ability exerted by G2 IgG. However, we demonstrated that G2 Fab can also prevent the binding of MERS-CoV S trimer with DPP4 despite no predicted steric clash between the G2 Fab and cell-surface DPP4 (Figure 5B). We also demonstrated that G2 Fab has the ability to prevent the attachment of soluble DPP4 to cell-surface S trimer (Figure 6). We feel it is unlikely that the reduced DPP4 binding can be attributed to steric interference with G2. It may be that there is some cross talk between the S1-NTDs and RBDs within the trimer, such that G2 binding to the NTDs reduces exposure of the RBDs in the receptor-accessible "up" conformation. A previous study identified a SARS-CoV S1-NTD-derived peptide (residues 217-234), designated "peptide 9626," that inhibits SARS-CoV S-mediated entry in a dose-dependent manner (Guo et al., 2009). When this peptide is mapped onto the cryo-EM structure of the SARS-CoV S trimer, it localizes to the S1-NTD-RBD interface, suggesting that the inhibition is mediated by interfering with the interaction between an S1-NTD and an RBD from an adjacent protomer.

Our data from the *in vitro* competition assay demonstrated that G2 Fab indirectly prevents the RBD-DPP4 interaction in the absence of any other attachment factors or co-receptors. However, several MERS-CoV attachment factors have been identified, including CEACAM5 (Chan et al., 2016), sialic acid (Li et al., 2017), and GRP78 (Chu et al., 2018). Several coronaviruses have been demonstrated to use the S1-NTD to bind glycans and the S1-CTD to bind the functional protein receptor (Li, 2015). In the case of TGEV, a porcine coronavirus, S1-NTD-mediated sialic acid binding is highly related to enteropathogenicity (Krempl et al., 1997). BCoV (Peng et al., 2012; Schultze et al., 1991) and OC43 (Künkel and Herrler, 1993) also use sialic acid as a receptor, with the sugar-binding pocket located on the S1-NTD top region. MHV, another β-coronavirus, uses the S1-NTD top region to bind its protein receptor CEACAM1 (Peng et al., 2011). Interestingly, although BCoV and MHV spikes bind to different host receptors, their S1-NTD binding surfaces are similarly presented (Figure 7), with the loop stretching out from β5 to β6 contributing most of the binding surface. G2-like antibodies may therefore directly block these receptor interactions for other coronaviruses.

As mentioned above, numerous S1-NTD-specific neutralizing antibodies have been isolated from mice, non-human primates (NHPs), and MERS-CoV patients (Chen et al., 2017; Wang et al., 2015, 2018), indicating that the S1-NTD is immunogenic. A recent study tested this directly by using a MERS-CoV S1-NTD fragment as an immunogen, and the results revealed that the S1-NTD can induce robust protective antibody responses in a mouse model (Jiaming et al., 2017). Our study defines a site of vulnerability on the S1-NTD, which may be important for structure-based vaccine design. Future efforts may improve the immunogenicity of the S1-NTD by exposing the vulnerable sites while masking or eliminating non-neutralizing epitopes, such as those normally buried in the prefusion spike. This strategy has already been successfully used for RBD-based vaccine

design (Du et al., 2016), wherein the introduction of glycosylation sites in the non-neutralizing epitopes led to an engineered RBD immunogen that was significantly more efficacious in a mouse model of MERS-CoV challenge.

STAR★METHODS

Detailed methods are provided in the online version of this paper and include the following:

- KEY RESOURCES TABLE
- LEAD CONTACT AND MATERIALS AVAILABILITY
- EXPERIMENTAL MODEL AND SUBJECT DETAILS
  - Cell Lines
  - Viral Strains
- METHOD DETAILS
  - Selection and Analysis of G2-Escape Variants
  - Plaque-Reduction Neutralization Assay
  - Pseudovirus Infectivity Experiments
  - Production of G2 Fab
  - Production of MERS-CoV S1-NTD and Mutants
  - Production of MERS-CoV S0 and S-2P
  - Production of MERS-CoV S-NTD Bound to G2 Fab
  - Crystallization and X-Ray Data Collection
  - X-Ray Structure Determination and Refinement
  - Production of MERS-CoV S0 Bound to G2 Fab
  - Negative-Stain Electron Microscopy
  - Cryo-EM Data Collection and Processing
  - Cryo-EM Model Generation
  - Surface Plasmon Resonance Affinity Assays
  - Flow Cytometry Using rDPP4-Expressing Cells
  - Flow Cytometry Using S-Expressing Cells
  - Image Cytometric Analysis
  - Neutralization Assay Comparing G2 IgG versus Fab
  - Surface Plasmon Resonance Competition Assay
- QUANTIFICATION AND STATISTICAL ANALYSIS
- DATA AND CODE AVAILABILITY

SUPPLEMENTAL INFORMATION

Supplemental Information can be found online at https://doi.org/10.1016/j.celrep.2019.08.052.

ACKNOWLEDGMENTS

We thank colleagues and members of our labs for comments on the manuscript, Emilie Shipman (Dartmouth College) and John Ludes-Meyers (UT-Austin) for assistance with protein expression, the beamline scientists for X-ray data collection support at SBC 19-ID (Argonne National Laboratory), Xiaotao Lu (Vanderbilt) for mutant virus construction using the MERS-CoV BAC, Erica Andres (Vanderbilt) and Xiaotao Lu for assistance with selection and sequence analysis of G2 escape-mutant viruses, and Gabriel Ozorowski for assistance with cryo-EM model building and refinement. This work was supported by NIH grant R01AI127521 (to J.S.M. and A.B.W.), NIH contract HHSN261200800001E agreement 16x142 (to M.R.D. and J.D.C.), and intramural funding from National Institute of Allergy and Infectious Diseases for work at the VRC (B.S.G.). Argonne is operated by UChicago Argonne, LLC, for the U.S. Department of Energy (DOE), Office of Biological and Environmental Research under contract DE-AC02-06CH11357.

AUTHOR CONTRIBUTIONS

N.W. designed and produced MERS-CoV S, S1-NTD, and G2 Fab proteins and different variants; crystallized G2 Fab and NTD–Fab complex and determined the structures; and conducted the SPR assay, cell-surface binding assay, and competition assay. O.R. and K.S.C. conducted the study to compare the efficacy of G2 Fab and IgG on binding inhibition and neutralization. L.W. conducted the neutralizing assay of G2 against pseudoviruses bearing MERS-CoV S, MERS-CoV S-S28F, and MERS-CoV S-G198D. W.S., Y.Z., and K.L. generated reagents used in multiple assays. H.L.T. performed the negative-stain EM study. J.P. collected the cryo-EM data and C.A.B. processed the data and determined the structure. M.M.B., J.D.C., and M.R.D. isolated and analyzed G2-escape variants of MERS-CoV. L.J.S., J.D.C., and M.R.D. conducted neutralization studies with authentic MERS-CoV (or MERS-CoV variants) in a BSL-3 setting. N.W., A.B.W., B.S.G, and J.S.M. conceived and designed the study and analyzed data. N.W. and J.S.M wrote the initial draft of the manuscript, on which all authors provided edits and comments.

DECLARATION OF INTERESTS

N.W., K.S.C., R.N.K., H.L.T., B.S.G., A.B.W., and J.S.M. are inventors on U.S. patent application 62/412,703, entitled "Prefusion Coronavirus Spike Proteins and Their Use." L.W., W.S., and B.S.G. are inventors on U.S. patent application PCT/US2016/019395, entitled "Middle East Respiratory Syndrome Coronavirus Immunogens, Antibodies and Their Use."

Received: February 6, 2019
Revised: June 6, 2019
Accepted: August 16, 2019
Published: September 24, 2019

REFERENCES

Adams, P.D., Grosse-Kunstleve, R.W., Hung, L.W., Ioerger, T.R., McCoy, A.J., Moriarty, N.W., Read, R.J., Sacchettini, J.C., Sauter, N.K., and Terwilliger, T.C. (2002). PHENIX: building new software for automated crystallographic structure determination. Acta. Crystallogr. D Biol. Crystallogr. *58*, 1948–1954.

Almazán, F., DeDiego, M.L., Sola, I., Zuñiga, S., Nieto-Torres, J.L., Marquez-Jurado, S., Andrés, G., and Enjuanes, L. (2013). Engineering a replication-competent, propagation-defective Middle East respiratory syndrome coronavirus as a vaccine candidate. MBio *4*, e00650-13.

Assiri, A.M., Midgley, C.M., Abedi, G.R., Bin Saeed, A., Almasri, M.M., Lu, X., Al-Abdely, H.M., Abdalla, O., Mohammed, M., Algarni, H.S., et al. (2016). Epidemiology of a Novel Recombinant Middle East Respiratory Syndrome Coronavirus in Humans in Saudi Arabia. J. Infect. Dis. *214*, 712–721.

Azhar, E.I., El-Kafrawy, S.A., Farraj, S.A., Hassan, A.M., Al-Saeed, M.S., Hashem, A.M., and Madani, T.A. (2014). Evidence for camel-to-human transmission of MERS coronavirus. N. Engl. J. Med. *370*, 2499–2505.

Battye, T.G., Kontogiannis, L., Johnson, O., Powell, H.R., and Leslie, A.G. (2011). iMOSFLM: a new graphical interface for diffraction-image processing with MOSFLM. Acta Crystallogr. D Biol. Crystallogr. *67*, 271–281.

Chan, C.M., Chu, H., Wang, Y., Wong, B.H., Zhao, X., Zhou, J., Yang, D., Leung, S.P., Chan, J.F., Yeung, M.L., et al. (2016). Carcinoembryonic Antigen-Related Cell Adhesion Molecule 5 Is an Important Surface Attachment Factor That Facilitates Entry of Middle East Respiratory Syndrome Coronavirus. J. Virol. *90*, 9114–9127.

Chen, Y., Lu, S., Jia, H., Deng, Y., Zhou, J., Huang, B., Yu, Y., Lan, J., Wang, W., Lou, Y., et al. (2017). A novel neutralizing monoclonal antibody targeting the N-terminal domain of the MERS-CoV spike protein. Emerg. Microbes Infect. *6*, e60.

Chu, H., Chan, C.M., Zhang, X., Wang, Y., Yuan, S., Zhou, J., Au-Yeung, R.K., Sze, K.H., Yang, D., Shuai, H., et al. (2018). Middle East respiratory syndrome coronavirus and bat coronavirus HKU9 both can utilize GRP78 for attachment onto host cells. J. Biol. Chem. *293*, 11709–11726.

Conway, P., Tyka, M.D., DiMaio, F., Konerding, D.E., and Baker, D. (2014). Relaxation of backbone bond geometry improves protein energy landscape modeling. Protein Sci. *23*, 47–55.

Corti, D., Zhao, J., Pedotti, M., Simonelli, L., Agnihothram, S., Fett, C., Fernandez-Rodriguez, B., Foglierini, M., Agatic, G., Vanzetta, F., et al. (2015). Prophylactic and postexposure efficacy of a potent human monoclonal antibody against MERS coronavirus. Proc. Natl. Acad. Sci. USA *112*, 10473–10478.

Coughlin, M.M., Babcook, J., and Prabhakar, B.S. (2009). Human monoclonal antibodies to SARS-coronavirus inhibit infection by different mechanisms. Virology *394*, 39–46.

Drosten, C., Muth, D., Corman, V.M., Hussain, R., Al Masri, M., HajOmar, W., Landt, O., Assiri, A., Eckerle, I., Al Shangiti, A., et al. (2015). An observational, laboratory-based study of outbreaks of middle East respiratory syndrome coronavirus in Jeddah and Riyadh, kingdom of Saudi Arabia, 2014. Clin. Infect. Dis. *60*, 369–377.

Du, L., Tai, W., Yang, Y., Zhao, G., Zhu, Q., Sun, S., Liu, C., Tao, X., Tseng, C.K., Perlman, S., et al. (2016). Introduction of neutralizing immunogenicity index to the rational design of MERS coronavirus subunit vaccines. Nat. Commun. *7*, 13473.

Emsley, P., and Cowtan, K. (2004). Coot: model-building tools for molecular graphics. Acta Crystallogr. D Biol. Crystallogr. *60*, 2126–2132.

Evans, P.R., and Murshudov, G.N. (2013). How good are my data and what is the resolution? Acta Crystallogr. D Biol. Crystallogr. *69*, 1204–1214.

Fehr, A.R., Athmer, J., Channappanavar, R., Phillips, J.M., Meyerholz, D.K., and Perlman, S. (2015). The nsp3 macrodomain promotes virulence in mice with coronavirus-induced encephalitis. J. Virol. *89*, 1523–1536.

Gierer, S., Bertram, S., Kaup, F., Wrensch, F., Heurich, A., Krämer-Kühl, A., Welsch, K., Winkler, M., Meyer, B., Drosten, C., et al. (2013). The spike protein of the emerging betacoronavirus EMC uses a novel coronavirus receptor for entry, can be activated by TMPRSS2, and is targeted by neutralizing antibodies. J. Virol. *87*, 5502–5511.

Greenough, T.C., Babcock, G.J., Roberts, A., Hernandez, H.J., Thomas, W.D., Jr., Coccia, J.A., Graziano, R.F., Srinivasan, M., Lowy, I., Finberg, R.W., et al. (2005). Development and characterization of a severe acute respiratory syndrome-associated coronavirus-neutralizing human monoclonal antibody that provides effective immunoprophylaxis in mice. J. Infect. Dis. *191*, 507–514.

Gui, M., Song, W., Zhou, H., Xu, J., Chen, S., Xiang, Y., and Wang, X. (2017). Cryo-electron microscopy structures of the SARS-CoV spike glycoprotein reveal a prerequisite conformational state for receptor binding. Cell Res. *27*, 119–129.

Guo, Y., Tisoncik, J., McReynolds, S., Farzan, M., Prabhakar, B.S., Gallagher, T., Rong, L., and Caffrey, M. (2009). Identification of a new region of SARS-CoV S protein critical for viral entry. J. Mol. Biol. *394*, 600–605.

Jiaming, L., Yanfeng, Y., Yao, D., Yawei, H., Linlin, B., Baoying, H., Jinghua, Y., Gao, G.F., Chuan, Q., and Wenjie, T. (2017). The recombinant N-terminal domain of spike proteins is a potential vaccine against Middle East respiratory syndrome coronavirus (MERS-CoV) infection. Vaccine *35*, 10–18.

Jiang, L., Wang, N., Zuo, T., Shi, X., Poon, K.M., Wu, Y., Gao, F., Li, D., Wang, R., Guo, J., et al. (2014). Potent neutralization of MERS-CoV by human neutralizing monoclonal antibodies to the viral spike glycoprotein. Sci. Transl. Med. *6*, 234ra59.

Ki, M. (2015). 2015 MERS outbreak in Korea: hospital-to-hospital transmission. Epidemiol. Health *37*, e2015033.

Kirchdoerfer, R.N., Cottrell, C.A., Wang, N., Pallesen, J., Yassine, H.M., Turner, H.L., Corbett, K.S., Graham, B.S., McLellan, J.S., and Ward, A.B. (2016). Pre-fusion structure of a human coronavirus spike protein. Nature *531*, 118–121.

Krempl, C., Schultze, B., Laude, H., and Herrler, G. (1997). Point mutations in the S protein connect the sialic acid binding activity with the enteropathogenicity of transmissible gastroenteritis coronavirus. J. Virol. *71*, 3285–3287.

Krissinel, E., and Henrick, K. (2007). Inference of macromolecular assemblies from crystalline state. J. Mol. Biol. *372*, 774–797.

Künkel, F., and Herrler, G. (1993). Structural and functional analysis of the surface protein of human coronavirus OC43. Virology *195*, 195–202.

Lander, G.C., Stagg, S.M., Voss, N.R., Cheng, A., Fellmann, D., Pulokas, J., Yoshioka, C., Irving, C., Mulder, A., Lau, P.W., et al. (2009). Appion: an integrated, database-driven pipeline to facilitate EM image processing. J. Struct. Biol. *166*, 95–102.

Li, F. (2015). Receptor recognition mechanisms of coronaviruses: a decade of structural studies. J. Virol. *89*, 1954–1964.

Li, F. (2016). Structure, Function, and Evolution of Coronavirus Spike Proteins. Annu. Rev. Virol. *3*, 237–261.

Li, F., Li, W., Farzan, M., and Harrison, S.C. (2005). Structure of SARS coronavirus spike receptor-binding domain complexed with receptor. Science *309*, 1864–1868.

Li, W., Moore, M.J., Vasilieva, N., Sui, J., Wong, S.K., Berne, M.A., Somasundaran, M., Sullivan, J.L., Luzuriaga, K., Greenough, T.C., et al. (2003). Angiotensin-converting enzyme 2 is a functional receptor for the SARS coronavirus. Nature *426*, 450–454.

Li, W., Hulswit, R.J.G., Widjaja, I., Raj, V.S., McBride, R., Peng, W., Widagdo, W., Tortorici, M.A., van Dieren, B., Lang, Y., et al. (2017). Identification of sialic acid-binding function for the Middle East respiratory syndrome coronavirus spike glycoprotein. Proc. Natl. Acad. Sci. USA *114*, E8508–E8517.

Li, Y., Wan, Y., Liu, P., Zhao, J., Lu, G., Qi, J., Wang, Q., Lu, X., Wu, Y., Liu, W., et al. (2015). A humanized neutralizing antibody against MERS-CoV targeting the receptor-binding domain of the spike protein. Cell Res. *25*, 1237–1249.

Lu, G., Hu, Y., Wang, Q., Qi, J., Gao, F., Li, Y., Zhang, Y., Zhang, W., Yuan, Y., Bao, J., et al. (2013). Molecular basis of binding between novel human coronavirus MERS-CoV and its receptor CD26. Nature *500*, 227–231.

McCoy, A.J., Grosse-Kunstleve, R.W., Adams, P.D., Winn, M.D., Storoni, L.C., and Read, R.J. (2007). Phaser crystallographic software. J. Appl. Cryst. *40*, 658–674.

Millet, J.K., and Whittaker, G.R. (2014). Host cell entry of Middle East respiratory syndrome coronavirus after two-step, furin-mediated activation of the spike protein. Proc. Natl. Acad. Sci. USA *111*, 15214–15219.

Modjarrad, K., Moorthy, V.S., Ben Embarek, P., Van Kerkhove, M., Kim, J., and Kieny, M.P. (2016). A roadmap for MERS-CoV research and product development: report from a World Health Organization consultation. Nat. Med. *22*, 701–705.

Mohd, H.A., Al-Tawfiq, J.A., and Memish, Z.A. (2016). Middle East Respiratory Syndrome Coronavirus (MERS-CoV) origin and animal reservoir. Virol. J. *13*, 87.

Nagae, M., Ikeda, A., Hane, M., Hanashima, S., Kitajima, K., Sato, C., and Yamaguchi, Y. (2013). Crystal structure of anti-polysialic acid antibody single chain Fv fragment complexed with octasialic acid: insight into the binding preference for polysialic acid. J. Biol. Chem. *288*, 33784–33796.

Naldini, L., Blömer, U., Gage, F.H., Trono, D., and Verma, I.M. (1996). Efficient transfer, integration, and sustained long-term expression of the transgene in adult rat brains injected with a lentiviral vector. Proc. Natl. Acad. Sci. USA *93*, 11382–11388.

Oboho, I.K., Tomczyk, S.M., Al-Asmari, A.M., Banjar, A.A., Al-Mugti, H., Aloraini, M.S., Alkhaldi, K.Z., Almohammadi, E.L., Alraddadi, B.M., Gerber, S.I., et al. (2015). 2014 MERS-CoV outbreak in Jeddah–a link to health care facilities. N. Engl. J. Med. *372*, 846–854.

Ogura, T., Iwasaki, K., and Sato, C. (2003). Topology representing network enables highly accurate classification of protein images taken by cryo electron-microscope without masking. J. Struct. Biol. *143*, 185–200.

Pallesen, J., Wang, N., Corbett, K.S., Wrapp, D., Kirchdoerfer, R.N., Turner, H.L., Cottrell, C.A., Becker, M.M., Wang, L., Shi, W., et al. (2017). Immunogenicity and structures of a rationally designed prefusion MERS-CoV spike antigen. Proc. Natl. Acad. Sci. USA *114*, E7348–E7357.

Peng, G., Sun, D., Rajashankar, K.R., Qian, Z., Holmes, K.V., and Li, F. (2011). Crystal structure of mouse coronavirus receptor-binding domain complexed with its murine receptor. Proc. Natl. Acad. Sci. USA *108*, 10696–10701.

Peng, G., Xu, L., Lin, Y.L., Chen, L., Pasquarella, J.R., Holmes, K.V., and Li, F. (2012). Crystal structure of bovine coronavirus spike protein lectin domain. J. Biol. Chem. *287*, 41931–41938.

Pettersen, E.F., Goddard, T.D., Huang, C.C., Couch, G.S., Greenblatt, D.M., Meng, E.C., and Ferrin, T.E. (2004). UCSF Chimera–a visualization system for exploratory research and analysis. J. Comput. Chem. *25*, 1605–1612.

Potter, C.S., Chu, H., Frey, B., Green, C., Kisseberth, N., Madden, T.J., Miller, K.L., Nahrstedt, K., Pulokas, J., Reilein, A., et al. (1999). Leginon: a system for fully automated acquisition of 1000 electron micrographs a day. Ultramicroscopy *77*, 153–161.

Potterton, E., Briggs, P., Turkenburg, M., and Dodson, E. (2003). A graphical user interface to the CCP4 program suite. Acta. Crystallogr. D Biol. Crystallogr. *59*, 1131–1137.

Punjani, A., Rubinstein, J.L., Fleet, D.J., and Brubaker, M.A. (2017). cryoSPARC: algorithms for rapid unsupervised cryo-EM structure determination. Nat. Methods *14*, 290–296.

Raj, V.S., Mou, H., Smits, S.L., Dekkers, D.H., Müller, M.A., Dijkman, R., Muth, D., Demmers, J.A., Zaki, A., Fouchier, R.A., et al. (2013). Dipeptidyl peptidase 4 is a functional receptor for the emerging human coronavirus-EMC. Nature *495*, 251–254.

Rockx, B., Corti, D., Donaldson, E., Sheahan, T., Stadler, K., Lanzavecchia, A., and Baric, R. (2008). Structural basis for potent cross-neutralizing human monoclonal antibody protection against lethal human and zoonotic severe acute respiratory syndrome coronavirus challenge. J. Virol. *82*, 3220–3235.

Rosen, O., Chan, L.L., Abiona, O.M., Gough, P., Wang, L., Shi, W., Zhang, Y., Wang, N., Kong, W.P., McLellan, J.S., et al. (2019). A high-throughput inhibition assay to study MERS-CoV antibody interactions using image cytometry. J. Virol. Methods *265*, 77–83.

Schultze, B., Gross, H.J., Brossmer, R., and Herrler, G. (1991). The S protein of bovine coronavirus is a hemagglutinin recognizing 9-O-acetylated sialic acid as a receptor determinant. J. Virol. *65*, 6232–6237.

Scobey, T., Yount, B.L., Sims, A.C., Donaldson, E.F., Agnihothram, S.S., Menachery, V.D., Graham, R.L., Swanstrom, J., Bove, P.F., Kim, J.D., et al. (2013). Reverse genetics with a full-length infectious cDNA of the Middle East respiratory syndrome coronavirus. Proc. Natl. Acad. Sci. USA *110*, 16157–16162.

Shang, J., Zheng, Y., Yang, Y., Liu, C., Geng, Q., Luo, C., Zhang, W., and Li, F. (2018a). Cryo-EM structure of infectious bronchitis coronavirus spike protein reveals structural and functional evolution of coronavirus spike proteins. PLoS Pathog. *14*, e1007009.

Shang, J., Zheng, Y., Yang, Y., Liu, C., Geng, Q., Tai, W., Du, L., Zhou, Y., Zhang, W., and Li, F. (2018b). Cryo-Electron Microscopy Structure of Porcine Deltacoronavirus Spike Protein in the Prefusion State. J. Virol. *92*, e01556-17.

Song, W., Gui, M., Wang, X., and Xiang, Y. (2018). Cryo-EM structure of the SARS coronavirus spike glycoprotein in complex with its host cell receptor ACE2. PLoS Pathog. *14*, e1007236.

Stewart, S.A., Dykxhoorn, D.M., Palliser, D., Mizuno, H., Yu, E.Y., An, D.S., Sabatini, D.M., Chen, I.S., Hahn, W.C., Sharp, P.A., et al. (2003). Lentivirus-delivered stable gene silencing by RNAi in primary cells. RNA *9*, 493–501.

Suloway, C., Pulokas, J., Fellmann, D., Cheng, A., Guerra, F., Quispe, J., Stagg, S., Potter, C.S., and Carragher, B. (2005). Automated molecular microscopy: the new Leginon system. J. Struct. Biol. *151*, 41–60.

Tang, G., Peng, L., Baldwin, P.R., Mann, D.S., Jiang, W., Rees, I., and Ludtke, S.J. (2007). EMAN2: an extensible image processing suite for electron microscopy. J. Struct. Biol. *157*, 38–46.

Tang, X.C., Agnihothram, S.S., Jiao, Y., Stanhope, J., Graham, R.L., Peterson, E.C., Avnir, Y., Tallarico, A.S., Sheehan, J., Zhu, Q., et al. (2014). Identification of human neutralizing antibodies against MERS-CoV and their role in virus adaptive evolution. Proc. Natl. Acad. Sci. USA *111*, E2018–E2026.

van Boheemen, S., de Graaf, M., Lauber, C., Bestebroer, T.M., Raj, V.S., Zaki, A.M., Osterhaus, A.D., Haagmans, B.L., Gorbalenya, A.E., Snijder, E.J., and Fouchier, R.A. (2012). Genomic characterization of a newly discovered coronavirus associated with acute respiratory distress syndrome in humans. MBio *3*, e00473-12.

Voss, N.R., Yoshioka, C.K., Radermacher, M., Potter, C.S., and Carragher, B. (2009). DoG Picker and TiltPicker: software tools to facilitate particle selection in single particle electron microscopy. J. Struct. Biol. *166*, 205–213.

Walls, A.C., Tortorici, M.A., Bosch, B.J., Frenz, B., Rottier, P.J.M., DiMaio, F., Rey, F.A., and Veesler, D. (2016a). Cryo-electron microscopy structure of a coronavirus spike glycoprotein trimer. Nature *531*, 114–117.

Walls, A.C., Tortorici, M.A., Frenz, B., Snijder, J., Li, W., Rey, F.A., DiMaio, F., Bosch, B.J., and Veesler, D. (2016b). Glycan shield and epitope masking of a coronavirus spike protein observed by cryo-electron microscopy. Nat. Struct. Mol. Biol. *23*, 899–905.

Walls, A.C., Xiong, X., Park, Y.J., Tortorici, M.A., Snijder, J., Quispe, J., Cameroni, E., Gopal, R., Dai, M., Lanzavecchia, A., et al. (2019). Unexpected Receptor Functional Mimicry Elucidates Activation of Coronavirus Fusion. Cell *176*, 1026–1039.e15.

Wang, L., Shi, W., Joyce, M.G., Modjarrad, K., Zhang, Y., Leung, K., Lees, C.R., Zhou, T., Yassine, H.M., Kanekiyo, M., et al. (2015). Evaluation of candidate vaccine approaches for MERS-CoV. Nat. Commun. *6*, 7712.

Wang, L., Shi, W., Chappell, J.D., Joyce, M.G., Zhang, Y., Kanekiyo, M., Becker, M.M., van Doremalen, N., Fischer, R., Wang, N., et al. (2018). Importance of Neutralizing Monoclonal Antibodies Targeting Multiple Antigenic Sites on the Middle East Respiratory Syndrome Coronavirus Spike Glycoprotein To Avoid Neutralization Escape. J. Virol. *92*, e02002-17.

Wang, N., Shi, X., Jiang, L., Zhang, S., Wang, D., Tong, P., Guo, D., Fu, L., Cui, Y., Liu, X., et al. (2013). Structure of MERS-CoV spike receptor-binding domain complexed with human receptor DPP4. Cell Res. *23*, 986–993.

WHO (2018). Middle East respiratory syndrome coronavirus (MERS-CoV) (World Health Organization). https://www.who.int/emergencies/mers-cov/en/.

Xiong, X., Tortorici, M.A., Snijder, J., Yoshioka, C., Walls, A.C., Li, W., McGuire, A.T., Rey, F.A., Bosch, B.J., and Veesler, D. (2018). Glycan Shield and Fusion Activation of a Deltacoronavirus Spike Glycoprotein Fine-Tuned for Enteric Infections. J. Virol. *92*, e01628-17.

Ying, T., Du, L., Ju, T.W., Prabakaran, P., Lau, C.C., Lu, L., Liu, Q., Wang, L., Feng, Y., Wang, Y., et al. (2014). Exceptionally potent neutralization of Middle East respiratory syndrome coronavirus by human monoclonal antibodies. J. Virol. *88*, 7796–7805.

Yuan, Y., Cao, D., Zhang, Y., Ma, J., Qi, J., Wang, Q., Lu, G., Wu, Y., Yan, J., Shi, Y., et al. (2017). Cryo-EM structures of MERS-CoV and SARS-CoV spike glycoproteins reveal the dynamic receptor binding domains. Nat. Commun. *8*, 15092.

Yusof, M.F., Queen, K., Eltahir, Y.M., Paden, C.R., Al Hammadi, Z.M.A.H., Tao, Y., Li, Y., Khalafalla, A.I., Shi, M., Zhang, J., et al. (2017). Diversity of Middle East respiratory syndrome coronaviruses in 109 dromedary camels based on full-genome sequencing, Abu Dhabi, United Arab Emirates. Emerg. Microbes Infect. *6*, e101.

Zaki, A.M., van Boheemen, S., Bestebroer, T.M., Osterhaus, A.D., and Fouchier, R.A. (2012). Isolation of a novel coronavirus from a man with pneumonia in Saudi Arabia. N. Engl. J. Med. *367*, 1814–1820.

Zhang, K. (2016). Gctf: Real-time CTF determination and correction. J. Struct. Biol. *193*, 1–12.

Zheng, S.Q., Palovcak, E., Armache, J.P., Verba, K.A., Cheng, Y., and Agard, D.A. (2017). MotionCor2: anisotropic correction of beam-induced motion for improved cryo-electron microscopy. Nat. Methods *14*, 331–332.

Zivanov, J., Nakane, T., Forsberg, B.O., Kimanius, D., Hagen, W.J., Lindahl, E., and Scheres, S.H. (2018). New tools for automated high-resolution cryo-EM structure determination in RELION-3. eLife *7*, e42166.

STAR★METHODS

KEY RESOURCES TABLE

REAGENT or RESOURCE	SOURCE	IDENTIFIER
Antibodies		
G2	Wang et al., 2015	N/A
G4	Wang et al., 2015	N/A
D12	Wang et al., 2015	N/A
JC57-14	Wang et al., 2018	N/A
Goat anti-human IgG, Alexa Fluor ® 647-conjugated	ThermoFisher Scientific	Cat#A-21445
Goat anti-rabbit IgG, Alexa Fluor® 488-conjugated	Abcam	Cat#ab150089
MERS-CoV S Antibody, Rabbit pAb	Sino Biological	Cat#40069
Bacterial and Virus Strains		
MERS-CoV EMC/2012	Scobey et al., 2013	N/A
MERS-CoV EMC/2012	Almazán et al., 2013	N/A
Chemicals, Peptides, and Recombinant Proteins		
Kifunensine	GlycoSyn	Cat#FC-034
DAPI	ThermoFisher Scientific	Cat#D1306
25 kDa linear polyethylenimine	Polysciences	Cat#3966-2
Fugene 6 transfection reagent	Promega	Cat#E2691
Lipofectamine 3000 reagent	ThermoFisher Scientific	Cat#L3000001
TRIzol reagent	ThermoFisher Scientific	Cat#15596026
MERS-CoV S-2P	Pallesen et al., 2017	N/A
MERS-CoV S0	This paper	N/A
MERS-CoV S-2P-GFP	This paper	N/A
Critical Commercial Assays		
Luciferase assay kit	Promega	Cat#E1501
Deposited Data		
G2 Fab structure	This paper	PDB: 6PXG
MERS-CoV S1-NTD–G2 Fab structure	This paper	PDB: 6PXH
Cryo-EM map of MERS-S0–G2 Fab complex	This paper	EMDB: EMD-20527
Coordinates for MERS-S0–G2 Fab complex	This paper	PDB: 6PZ8
Experimental Models: Cell Lines		
FreeStyle 293-F Cells	ThermoFisher Scientific	Cat#R79007
Expi293F Cells	ThermoFisher Scientific	Cat#A14527
Vero 81 cells	ATCC	CCL-81
293T cells	ATCC	CRL-11268
BHK-21 cells	ATCC	CCL-10 TM
Huh7.5 cells	Provided by Dr. Deborah R. Taylor of the US FDA	N/A
Recombinant DNA		
pCMVDR8.2	Stewart et al., 2003	Addgene Cat#8455
pHR′ CMV-Luc	Barney Graham Laboratory	N/A
CMV/R-MERS-CoV S	Barney Graham Laboratory	N/A
pαH expression plasmid	Jason McLellan Laboratory	N/A
pVRC8400 expression plasmid	Barney Graham Laboratory	N/A
pαH-S1-TM	This paper	N/A
pαH-S-WT-FL	This paper	N/A

(*Continued on next page*)

Continued

REAGENT or RESOURCE	SOURCE	IDENTIFIER
pαH-S-2P-FL	This paper	N/A
pαH-DPP4	This paper	N/A
paH-DPP4-ECD-HSS	This paper	N/A
Software and Algorithms		
Prism (V7)	GraphPad	RRID: SCR_002798
FlowJo (V7.6.1)	FlowJo	RRID: SCR_008520
Scrubber2	BioLogic	RRID: SCR_015745
cryoSPARC v2	Punjani et al., 2017	RRID: SCR_016501
Pymol	Schrödinger	RRID: SCR_000305
UCSF Chimera	Pettersen et al., 2004	RRID: SCR_004097
CCP4i interface	Potterton et al., 2003	http://www.ccp4.ac.uk
PHASER	McCoy et al., 2007	RRID: SCR_014219
COOT	Emsley and Cowtan, 2004	RRID: SCR_014222
Phenix	Adams et al., 2002	RRID: SCR_014224
Leginon software suite	Potter et al., 1999	RRID: SCR_016731
Appion	Lander et al., 2009	RRID: SCR_016734
EMAN2	Tang et al., 2007	RRID: SCR_016867
Rosetta (v2019.14.60699)	Conway et al., 2014	RRID: SCR_015701
PISA	Krissinel and Henrick, 2007	RRID: SCR_015749
MotionCor2	Zheng et al., 2017	RRID: SCR_016499
GCTF	Zhang, 2016	RRID: SCR_016500
DoG Picker	Voss et al., 2009	RRID: SCR_016655
Other		
Strep-Tactin Superflow resin	IBA Lifesciences	Cat# 2-1206-010
Biacore Sensor Chip NTA	GE Healthcare	Cat#BR100407
Biacore Sensor Chip NTA CM5	GE Healthcare	Cat# BR100399
Protein A agarose	ThermoFisher Scientific	Cat#20334
HiLoad 16/600 Superdex 75 pg column	GE Healthcare	Cat#28989333
HiLoad 16/600 Superdex 200 pg column	GE Healthcare	Cat#28989335

LEAD CONTACT AND MATERIALS AVAILABILITY

Further information and requests for resources and reagents should be directed to and will be fulfilled by the Lead Contact, Jason S. McLellan (jmclellan@austin.utexas.edu). Reagents generated in this study are available via material transfer agreement (MTA).

EXPERIMENTAL MODEL AND SUBJECT DETAILS

Cell Lines

FreeStyle 293F cells and Expi293 cells were purchased from Thermofisher Scientific and used to express proteins, Fabs and IgGs. They are maintained following the company's protocol.

Vero 81 cells were obtained from ATCC, cultured in Dulbecco's Modified Eagle Medium (supplemented with 10% fetal bovine serum, 100 U/ml penicillin, 100 μg/ml streptomycin, and 0.25 μg/ml amphotericin B) in a humidified 37 °C incubator containing 5% CO_2, and used for *in vitro* selection of G2-escape variants and plaque-reduction neutralization assay.

HEK293T cells were obtained from ATCC, cultured in DMEM with 10% heat-inactivated fetal bovine serum (HI-FBS) and 1 × penicillin/streptomycin in a 37 °C incubator containing 5% CO_2, and used to produce MERS-CoV pseudoviruses.

BHK-21 cells were obtained from ATCC, cultured in DMEM medium with 10% HI-FBS and 1 × penicillin/streptomycin in a 37 °C incubator containing 5% CO_2.

Huh7.5 cells were provided by Dr Deborah R. Taylor of the US FDA and cultured in DMEM with 10% HI-FBS and 1 × penicillin/streptomycin in a 37 °C incubator containing 5% CO_2.

BHK-21 and Huh7.5 cells were used for neutralization assays in different experiments.

Viral Strains

Recombinant MERS-CoV strain EMC/2012 (Scobey et al., 2013) was used for selection of G2-escape variants. For plaque-reduction neutralization testing, recombinant wild-type and spike mutant MERS-CoV were recovered from a bacterial artificial chromosome (BAC) containing the full-length EMC/2012 isolate genome (Almazán et al., 2013), a gift from Dr. Stanley Perlman (University of Iowa). The G198D spike mutation, which arose during passage selection of MERS-CoV for resistance to G2-mediated neutralization, was introduced into the MERS-CoV BAC using published protocols (Fehr et al., 2015). The complete S gene sequence of recombinant virus was determined to confirm accuracy of mutagenesis.

METHOD DETAILS

Selection and Analysis of G2-Escape Variants

A P0 stock of recombinant MERS-CoV EMC/2012 recovered from an infectious clone (Scobey et al., 2013) was serially passaged in Vero 81 cells supplemented with increasing concentrations of G2. Three parallel passage series were performed. Passages were initiated at a multiplicity of infection (MOI) ~0.001 PFU per cell and G2 concentration = 0.43 μg/ml, corresponding to 0.75x G2 IC80 versus MERS-CoV in a plaque-reduction neutralization assay. Culture supernatants were passed onto fresh cells when 50%–60% of the monolayer displayed viral CPE. Viral inoculum volume and G2 concentrations were empirically co-adjusted between passage steps to produce the target CPE level at approximately 48 hours-post-infection (hpi). The G2 concentration at terminal passage, P10, was 0.65 μg/ml, corresponding to 11.2x IC80. 15 clonal escape mutant viruses (five from each passage) were isolated from P10 cultures via plaque purification on Vero 81 cells in the presence of 0.65 μg/ml G2. Viral plaques were expanded in Vero 81 cells, and total RNA was harvested in TRIzol reagent (Invitrogen), followed by RT-PCR to generate overlapping cDNA amplicons spanning the entire S gene open reading frame. PCR products were subjected to dideoxy sequencing, and reads were aligned to the native EMC/2012 S gene sequence (GenBank accession number JX869059.2) to identify differences. In a separate virus passage experiment, three parallel lineages of antibody-free P10 EMC/2012 cultures were examined for S mutations to identify cell culture-adaptive changes resulting from serial MERS-CoV passage. These substitutions were excluded from analysis of changes in S identified in G2 escape mutant isolates.

Plaque-Reduction Neutralization Assay

Wild-type and spike mutant MERS-CoV were recovered from a bacterial artificial chromosome (BAC) containing the full-length EMC/2012 isolate genome (Almazán et al., 2013), a gift from Dr. Stanley Perlman (University of Iowa). The G198D spike mutation, which arose during passage selection of MERS-CoV for resistance to G2-mediated neutralization, was introduced into the MERS-CoV BAC using published protocols (Fehr et al., 2015). The complete S gene sequence of recombinant virus was determined to confirm accuracy of mutagenesis.

Serial 2- or 10-fold dilutions of G2 IgG or Fab were combined with approximately 70–130 PFU of WT or G198D mutant MERS-CoV in a total volume of 200 μL gelatin saline (0.3% [wt/vol] gelatin in phosphate-buffered saline supplemented with $CaCl_2$ and $MgCl_2$). Virus-antibody mixtures were incubated for 20 min at 37°C, followed by adsorption of 100 μL aliquots to each of two confluent wells of Vero 81 cells in 6-well (10-cm^2) plates for 30 min at 37°C. Monolayers were overlaid with Dulbecco's modified Eagle's medium (DMEM) containing 1% agar, and plaques were enumerated at 96 h post-infection. Percent neutralization was calculated as average plaques produced by IgG- or Fab-treated virus divided by average plaques produced by virus in antibody-free gelatin saline.

Pseudovirus Infectivity Experiments

The S28F and G198D substitutions were introduced via PCR into a plasmid encoding full-length spike (MERS-CoV England1 AFY 13307). S-containing lentiviral pseudovirions (Eng1, Eng1-S28F and Eng1-G198D) were produced by co-transfection of three plasmids (packaging plasmid pCMVDR8.2, transducing plasmid pHR′ CMV-Luc, and CMV/R-MERS-CoV S plasmid) into 293T cells using Fugene 6 transfection reagent (Promega, Madison, WI) (Naldini et al., 1996). For the neutralization assay, Huh7.5 cells, provided by Deborah R. Taylor of the U.S. FDA, were plated into 96-well white/black Isoplates (PerkinElmer, Waltham, MA) at 10,000 cells/well the day before infection. Serial dilutions of monoclonal antibody were mixed with titrated pseudovirus, incubated for 30 min at 37°C, and added to Huh7.5 cells in triplicate. Following 2 h of incubation, wells were replenished with 100 μL of fresh medium. Cells were lysed 72 h later, and luciferase activity was measured. Percent neutralization was calculated from luminometry data.

Production of G2 Fab

The Fab region of the G2 heavy chain was fused with the HRV3C cleavage site followed by human IgG1 Fc fragment and subcloned into the eukaryotic expression vector pVRC8400. This plasmid (plasmid 1) was cotransfected with a vector encoding the G2 light chain (plasmid 2) into Expi293 cells (Invitrogen), and the secreted antibody was purified using Protein A agarose (Fisher). HRV3C protease (1% wt/wt) was added to the protein and the reaction was incubated for 2 h at room temperature. The digested antibody was passed back over Protein A agarose to remove the Fc fragment, and the unbound Fab was additionally purified using a Superdex 75 column (GE Healthcare).

Production of MERS-CoV S1-NTD and Mutants

A gene encoding MERS-CoV S1-NTD (residues 1–351) with a C-terminal HRV3C cleavage site, 8xHis-tag and Twin-Strep-tag was inserted into the eukaryotic expression vector pαH (plasmid 3). Three hours after transient transfection of the plasmid into FreeStyle 293-F cells, kifunensine was added to a final concentration of 5 μM. After 6 d, supernatant was filtered and passed over a Strep-Tactin column (IBA). The column was washed with PBS, and the S1-NTD was eluted by incubating the resin with HRV3C (1% wt/wt). The S1-NTD was further purified using a Superdex 200 column (GE Healthcare). S1-NTD mutants were expressed and purified using the same method.

Mutations were introduced into the S1-NTD fragment by overlapping PCR. To produce deglycosylated S1-NTD protein, EndoH (10% wt/wt) was added together with HRV3C (1% wt/wt) after the binding of protein onto a Strep-Tactin column.

Production of MERS-CoV S0 and S-2P

A mammalian-codon-optimized gene encoding MERS-CoV S (England1 strain) residues 1–1291 with a C-terminal T4 fibritin trimerization domain, HRV3C cleavage site, 8xHis-tag and Twin-Strep-tag was synthesized and subcloned into the eukaryotic-expression vector pαH. The S1/S2 furin-recognition site 748-RSVR-751 was mutated to ASVG to produce a single-chain MERS-S0 protein (plasmid 4). Two proline mutations, D1059P and V1060P, were introduced to S0 to generate a stabilized MERS-CoV S-2P protein (plasmid 5). Additional mutations were introduced into MERS-CoV S-2P to make MERS-CoV S-2P variants including S-2P-S28F and S-2P-G198D.

For expression, 0.5–1 L FreeStyle 293-F cells were transfected. Three hours after transfection, kifunensine was added to a final concentration of 5 μM. Cultures were harvested after 6 d, and protein was purified from the supernatant using Strep-Tactin resin (IBA). HRV3C protease (1% wt/wt) was added to the protein, and the reaction was incubated overnight at 4°C. Digested protein was further purified using a Superose 6 16/70 column (GE Healthcare).

Production of MERS-CoV S-NTD Bound to G2 Fab

Different methods to produce the S1-NTD–G2 Fab complex were tested to obtain crystals, involving different S1-NTD truncations, deglycosylation strategies, co-expression and co-purification strategies. High-quality crystals were only produced by co-transfection of S1-NTD and G2 in the presence of kifunensine, yet without any glycosidase treatment, as described in more detail below.

The three plasmids encoding G2 heavy chain (plasmid 1), G2 light chain (plasmid 2) and S1-NTD (plasmid 3) were co-transfected into FreeStyle 293-F cells. Three hours after transient transfection, kifunensine was added to a final concentration of 5 μM. After 6 d, supernatant was passed over a Protein A agarose column. The column was washed with PBS, and the complex was eluted by incubating resin with HRV3C (1% wt/wt). The sample was further purified using a Superdex 200 column (GE Healthcare).

Crystallization and X-Ray Data Collection

Crystals of G2 Fab were produced by hanging-drop vapor diffusion by mixing 1 μL of G2 Fab (11.5 mg/mL) with 1 μL of reservoir solution containing 15% ethanol and 40% pentaerythritol propoxylate (5/4 PO/OH). Crystals were soaked in reservoir solution supplemented with 25% (v/v) glycerol and frozen in liquid nitrogen. Diffraction data were collected at the SBC beamline 19-ID (Advanced Photon Source, Argonne National Laboratory).

Crystals of the complex of MERS-CoV S1-NTD with G2 Fab were produced by hanging-drop vapor diffusion by mixing 1 μL of protein (9.1 mg/mL) with 1 μL of reservoir solution containing 0.1 M imidazole pH 6.5, 0.2 M Li_2SO_4, 19% polyethylene glycol (PEG) 3350, and 6% 2-methyl-2,4-pentanediol (MPD). Crystals were soaked in reservoir solution supplemented with 20% (v/v) ethylene glycol and frozen in liquid nitrogen. Diffraction data were collected at the SBC beamline 19-ID (Advanced Photon Source, Argonne National Laboratory).

X-Ray Structure Determination and Refinement

Diffraction data were processed using the CCP4 software suite (Potterton et al., 2003): data were indexed and integrated in iMOSFLM (Battye et al., 2011) and scaled and merged with AIMLESS (Evans and Murshudov, 2013). A molecular replacement solution for the 2.1 Å G2 Fab dataset was found by PHASER (McCoy et al., 2007) using the variable and constant domains of PDB ID: 3WBD (Nagae et al., 2013) and PDB ID: 5VZR (Pallesen et al., 2017), respectively, as search models. The structure was built manually in COOT (Emsley and Cowtan, 2004) and refined using PHENIX (Adams et al., 2002).

A molecular replacement solution for the S1-NTD–G2 complex was obtained using PHASER with MERS-CoV S1-NTD (PDB ID: 5VYH (Pallesen et al., 2017)) and the solved G2 Fab structure as search models. There are two S1-NTD–G2 Fab complexes in each asymmetric unit (ASU). Model building was performed in COOT and refinement was performed in PHENIX. Data collection and refinement statistics for both structures are presented in Table S2.

Production of MERS-CoV S0 Bound to G2 Fab

Three plasmids (plasmids 1, 2 and 4) were co-transfected into FreeStyle 293-F cells. Three hours after transient transfection, kifunensine was added to a final concentration of 5 μM. After 6 d, supernatant was passed over a Protein A agarose column. The column was washed with PBS and the complex was eluted by incubating resin with HRV3C (1% wt/wt). The sample was further purified using a Superose 6 16/70 column (GE Healthcare).

Negative-Stain Electron Microscopy

Purified MERS-CoV S0–G2 Fab complex was added to carbon-coated 400 mesh copper grids and stained with 2% uranyl formate. Negative stain EM data was collected on a Tecnai Spirit operating at 120 kV with a 4k x 4k TemCam F416 camera. Micrographs were imaged through Leginon (Potter et al., 1999) and processed in Appion (Lander et al., 2009). Particles were selected using DoG picker (Voss et al., 2009), stacked, and 2D classes were produced by MSA/MRA (Ogura et al., 2003). The final 3D map was generated with EMAN2 (Tang et al., 2007).

Cryo-EM Data Collection and Processing

MERS-CoV S0–G2 complex was imaged on a Titan Krios operating at 300 kV using Leginon (Potter et al., 1999; Suloway et al., 2005). Each micrograph movie was collected at a magnification of 29,000x, resulting in a pixel size of 0.51 Å/pixel. Micrograph movies were recorded on a Gatan K2 detector in super-resolution mode. The dose rate was 2.50 e^-/pixel/s and the defocus range was 0.5–3.5 μm. Movie frames were aligned and dose-weighted using MotionCor2 (Zheng et al., 2017) and CTF models were calculated using GCTF (Zhang, 2016). A small subset of particles were picked using RELION's LoG Picker (Zivanov et al., 2018), which in turn were used to prepare templates for the template picker in cryoSPARC 2 (Punjani et al., 2017), resulting in 490,790 particles. 2D classification was used to clean junk particles and a clean particle stack submitted to 2-class *ab initio* refinement in cryoSPARC 2. The class representing the structure was used to perform one additional 2D classification step resulting in 5 templates. These templates were then used to pick particles on the original dataset resulting in 418,781 particles. The extracted particles were binned by a factor of 2. These particles were then subjected to an iterative process of filtering based on 2 class *ab initio* model refinement. Finally, homogeneous 3D refinement with sharpening in cryoSPARC 2 performed with a subset of 12,386 particles resulted in a 4.19 Å resolution reconstruction. Local resolution analysis performed in the latest version of cryoSPARC 2 of the map revealed a 4.44 Å resolution. Data collection and processing statistics are presented in Table S3.

Cryo-EM Model Generation

A previously published structure of MERS-CoV S (PDB ID: 5w9i) (Pallesen et al., 2017) exhibited a good fit into our map. We then aligned the model from the NTD-G2 crystal structure to the NTD domains of PDB 5w9i, which also exhibited a good fit except for the constant region of the G2 Fab which is typically flexible. We therefore deleted the constant region from the model. We also deleted the NTDs from 5w9i in favor of the higher resolution NTD from the NTD-G2 crystal structure. Given the resolution of our map, in particular the lower resolution of the NTD-G2 portion, we only conducted a light refinement in Rosetta (v2019.14.60699) (Conway et al., 2014) using the relax function (with constrain_relax_to_start_coords) to alleviate sidechain clashes in the hybrid model.

Surface Plasmon Resonance Affinity Assays

A Biacore X100 (GE Healthcare) was used to measure the binding of G2 Fab to immobilized MERS-CoV S1-NTD, S1-NTD mutants, S-2P or S-2P mutants. S1-NTD or S1-NTD mutants with an 8xHis-tag and Twin-Strep-tag were immobilized on a Ni-NTA sensor chip to a total of 80–120 response units. The chip was regenerated between each cycle using 0.35 M EDTA followed by 0.5 mM $NiCl_2$. A buffer-only sample was injected over the ligand-bound and reference flow cells, followed by G2 Fab serially diluted 2.5-fold in HBS-P^+ starting at 500 nM. Data were double-reference subtracted and fit to a 1:1 binding model using the Scrubber2 analysis software. To measure binding of G2 Fab to MERS-CoV S-2P or MERS-CoV S-2P mutants, similar experiments were performed, except that the S protein was immobilized to a total of 350–450 response units. All assays were performed at 25°C.

Flow Cytometry Using rDPP4-Expressing Cells

MERS-CoV S-2P (or the S28F or G198D mutants) was fused with a C-terminal HRV3C cleavage site, a GFP tag, an 8xHis-tag and a Strep-tag II, and subcloned into the vector pαH. Proteins were expressed in FreeStyle 293-F cells and purified using Strep-Tactin column.

FreeStyle 293-F cells were transfected with plasmids expressing full-length DPP4. 60 h after transfection, cells were harvested and washed twice with blocking buffer (PBS buffer supplemented with 0.5% BSA and 2 mM EDTA). Cells were then incubated with GFP-tagged S protein (or S variants, 200 nM) or GFP-tagged S protein (or S variants, 200 nM) supplemented with G2 or D12 or AM14 IgG (1 μM) for 30 min at 37°C. Cells were then washed twice with blocking buffer and subsequently stained with SYTOX Blue Dead Cell Stain (1:2000, ThermoFisher) before analysis using a MACSQuant VYB (Miltenyi Biotec). Data were analyzed with FlowJo software (Tree Star Inc.) using the following gating strategy: size & granularity → live cells (SYTOX Blue negative) → binding signal (GFP positive).

Flow Cytometry Using S-Expressing Cells

Human DPP4 ectodomain (residues 39–766) was fused with an artificial signal peptide (MRPTWAWWLFLVLLLALWAPARG) at the N terminus, and a HRV3C cleavage site, 8xHis tag and Twin-Strep tag at the C terminus, followed by subcloning into the vector pαH. Protein designated as DPP4-ECD-HSS was expressed in FreeStyle 293-F cells and purified using a Strep-Tactin column.

MERS-CoV S1 (residues 1–751) was fused with the RSV F transmembrane motif and subcloned into the vector pαH to generate the plasmid pαH-S1-TM. Full-length MERS-CoV S-WT or the stabilized S variant MERS-CoV S-2P was subcloned into the vector pαH to generate the plasmids pαH-S-WT-FL and pαH-S-2P-FL, respectively. FreeStyle 293-F cells were transfected and then harvested after 60 h to obtain S1-TM$^+$, S-WT-FL$^+$ and S-2P-FL$^+$ cells.

S1-TM$^+$, S-WT-FL$^+$ and S-2P-FL$^+$ cells were then washed twice with blocking buffer (PBS buffer supplemented with 0.5% BSA and 2 mM EDTA) and subsequently incubated with 100 nM DPP4-ECD-HSS with 200 nM anti-strep antibody (produced in-house) in the presence or absence of 500 nM G2 or G4 or JC57-14 Fab for 30 min at room temperature. Cells were washed, and a 1:500 dilution of Alexa Fluor^{TM} 647 goat anti-human IgG (H+L) (Invitrogen) was added and incubated for 30 min. Cells were then washed twice with blocking buffer and subsequently stained with SYTOX Blue Dead Cell Stain (1:2000, ThermoFisher) before analysis using a LSRFortessa SORP Flow Cytometer (BD). Data were analyzed with FlowJo software (Tree Star Inc.) using the following gating strategy: size & granularity → live cells (SYTOX Blue negative) → binding signal (Alexa Fluor^{TM} 647 positive).

Image Cytometric Analysis

Image cytometry methods were performed as previously described (Rosen et al., 2019). Briefly, BHK-21 cells were seeded into flat bottom black-walled Greiner 96-well plates and allowed to adhere overnight. On the following day, a DPP4 expression plasmid was transfected into the cells, using Lipofectamine 3000 reagent. Two days following DPP4 transfection, MERS-CoV S-2P was incubated with 4-fold serial dilutions of antibody (Fab or IgG) for 30 min at room temperature (RT). The mixture of MERS-CoV S and antibody was then added to the DPP4-expressing BHK-21 cells and incubated for 2 hours at RT. After incubation, cells were washed, fixed with 80% cold acetone, and rewashed. Subsequently, cells were stained with MERS-CoV S rabbit polyclonal antibodies (Sino Biological, Beijing, China) and then secondary goat anti-rabbit IgG H&L labeled with Alexa Fluor® 488 (AF488) was added. Finally, cell nuclei were stained with DAPI. Percent inhibition as a function of antibody concentrations was then plotted and analyzed via a one-site-fit Log IC_{50} non-linear regression analysis. No inhibition (0%) was defined as MERS-CoV S binding to BHK-21 cells without the addition of antibody. Full inhibition (100%) was defined as MERS-CoV S binding to BHK-21 without DPP4 receptor.

Neutralization Assay Comparing G2 IgG versus Fab

MERS-CoV (England1 strain) pseudovirions, expressing wild-type and mutant S proteins, were produced by co-transfection of three plasmids into 293T cells using Fugene 6 transfection reagent (Promega, Madison, WI) and titered, as described previously (Wang et al., 2018). For the neutralization assay, BHK-21 cells with exogenously expressed DPP4 were used as previously described (Rosen et al., 2019). Briefly, DPP4 was expressed in BHK-21 cells and two days post-transfection, antibodies were mixed with MERS-CoV pseudoviruses and added to cells. 72 hours later, cells were lysed and analyzed for luciferase activity. Relative luciferase units were measured and percent neutralization was calculated considering uninfected cells as 100% neutralization and cells transduced with only pseudovirus as 0% neutralization.

Surface Plasmon Resonance Competition Assay

A Biacore X100 (GE Healthcare) was used to measure the binding of un-tagged MERS-CoV S-2P—alone or in the presence of a 5-fold molar excess of IgG or Fab—to immobilized twin-Strep-tagged DPP4 ectodomain (DPP4-ECD-HSS). DPP4-ECD-HSS was captured using an anti-Strep antibody-coupled CM5 chip to a total of 65–75 response units. The chip was regenerated between each cycle using 10 mM glycine, pH 2.0 followed by 0.1% SDS. HBS-P$^+$ pH 8.0 was used for running buffer as well as sample buffer. For each cycle, HBS P$^+$ pH 8.0 was injected once after immobilization to further clean the chip, followed by the injection of buffer only, 500 nM Fab or IgG only, 100 nM S-2P only, or 100 nM S-2P supplemented with 500 nM Fab or IgG. Experiments were performed at 25°C. Data were reference-subtracted and analyzed in BIAevaluation software.

QUANTIFICATION AND STATISTICAL ANALYSIS

Binding and neutralization assays were conducted with at least duplicate measurements and presented as the mean ± SEM of the indicated number of replicates. Details can be found in figure legends.

DATA AND CODE AVAILABILITY

Coordinates and structure factors for G2 Fab have been deposited in the Protein Data Bank under accession code PDB: 6PXG. Coordinates and structure factors for MERS-CoV S1-NTD–G2 Fab have been deposited in the Protein Data Bank under accession code PDB: 6PXH. Cryo-EM reconstruction of MERS-S0–G2 Fab complex has been deposited in the Electron Microscopy Data Bank (EMDB) (accession code EMDB: EMD-20527). Atomic models have been deposited in the Protein Data Bank (PDB: 6PZ8).